Am J Nucl Med Mol Imaging 2024;14(1):1-12
www.ajnmmi.us /ISSN:2160-8407/ajnmmi0153988

Original Article

In vitro evaluation of PET radiotracers for imaging synaptic density, the acetylcholine transporter, AMPA-tarp-γ8 and muscarinic M4 receptors in Alzheimer's disease

Faustine d'Orchymont[1], Andrea Narvaez[1,2], Roger Raymond[1], Pallavi Sachdev[3], Arnaud Charil[3], Stephen Krause[3], Neil Vasdev[1,4]

[1]Azrieli Centre for Neuro-Radiochemistry, Brain Health Imaging Centre, Centre for Addiction and Mental Health (CAMH), Toronto, ON, Canada; [2]Enigma Biomedical Group, Inc., Toronto, ON, Canada; [3]Eisai, Inc., Nutley, NJ, USA; [4]Department of Psychiatry, University of Toronto, Toronto, ON, Canada

Received October 18, 2023; Accepted February 4, 2024; Epub February 20, 2024; Published February 28, 2024

Abstract: Several therapeutics and biomarkers that target Alzheimer's disease (AD) are under development. Our clinical positron emission tomography (PET) research programs are interested in six radiopharmaceuticals to image patients with AD and related dementias, specifically [^{11}C]UCB-J and [^{18}F]SynVesT-1 for synaptic vesicle glycoprotein 2A as a marker of synaptic density, two vesicular acetylcholine transporter PET radiotracers: [^{18}F]FEOBV and [^{18}F]VAT, as well as the transmembrane AMPA receptor regulatory protein (TARP)-γ8 tracer, [^{18}F]JNJ-64511070, and the muscarinic acetylcholine receptor (mAChR) M4 tracer [^{11}C]MK-6884. The goal of this study was to compare all six radiotracers (labeled with tritium or ^{18}F) by measuring their density variability in pathologically diagnosed cases of AD, mild cognitive impairment (MCI) and normal healthy volunteer (NHV) human brains, using thin-section *in vitro* autoradiography (ARG). Region of interest analysis was used to quantify radioligand binding density and determine whether the radioligands provide a signal-to-noise ratio optimal for showing changes in binding. Our preliminary study confirmed that all six radiotracers show specific binding in MCI and AD. An expected decrease in their respective target density in human AD hippocampus tissues compared to NHV was observed with [^{3}H]UCB-J, [^{3}H]SynVesT-1, [^{3}H]JNJ-64511070, and [^{3}H]MK-6884. This preliminary study will be used to guide human PET imaging of SV2A, TARP-γ8 and the mAChR M4 subtype for imaging in AD and related dementias.

Keywords: Autoradiography, glutamatergic, synaptic density, SV2A, SynVesT-1, cholinergic, fluorine-18, tritium, PET, Alzheimer's disease

Introduction

Losses of neurons, alterations of synapses and neurotransmission deficits are associated with many neurodegenerative disorders including Alzheimer's disease (AD). The loss of synaptic integrity observed in the brain of AD patients, especially in the frontal cortex and hippocampus regions, has been shown to be an important hallmark of AD, and leads to the downregulation of several presynaptic and postsynaptic proteins [1]. As a result, several efforts have been made to evaluate different targets in the brain and develop high-affinity and brain-penetrant positron emission tomography (PET) radiotracers to quantify changes in both normal and pathological conditions in AD. This study focused on four brain targets: the synaptic vesicle glycoprotein 2 (SV2A), the vesicular acetylcholine transporter (VAChT), the transmembrane AMPA receptor regulatory protein (TARP)-γ8, and the M4 subtype of muscarinic acetylcholine (ACh) receptors which play a crucial role in neurotransmission as their altered expression strongly correlates with severity of AD pathologies.

As one of the membrane proteins on the synaptic vesicles, expressed in high concentration throughout the brain, SV2A is vital to neurotransmission and has been of major interest to detect reduced synaptic density in living patients with AD pathologies using PET [2-4]. A first-generation SV2A radiotracer for PET is [^{11}C]UCB-J (**Figure 1**), which showed high specific binding signals and high binding kinetics in the human brain and was validated as a viable biomarker for synaptic density imaging [5-7]. With the increased efforts invested in the development of ^{18}F-labeled analogues of UCB-J for widespread human translation, [^{18}F]SynVesT-1 (Scheme 1, also known as [^{18}F]SDM-8 or [^{18}F]MNI-1126) was developed as a promising SV2A biomarker, presenting similar pharmacokinetics as [^{11}C]UCB-J, with the advantages of ^{18}F-labeling [4, 8, 9].

Located in presynaptic terminal vesicles of cholinergic neurons, VAChT regulates the synthesis and release of acetylcholine [10]. Degeneration of cholinergic cells in the brain have been shown to correlate with AD pathologies and perturbs cholinergic neurotransmission in the cortex and hippocampus [11, 12]. Thus, the quantification of VAChT by PET has been established as a potential tool for diagnosis of AD [13-17]. Vesamicol and derivatives have been evaluated as specific ligands for VAChT [18-20]. Despite efforts focused on optimizing the chemical structure to increase the selectivity, *in vivo* kinetics, and metabolic stability, only a few ^{11}C- and ^{18}F-labeled ligands have progressed to PET imaging of non-human primate and human subjects [21-24]. Two promising PET radiopharma-

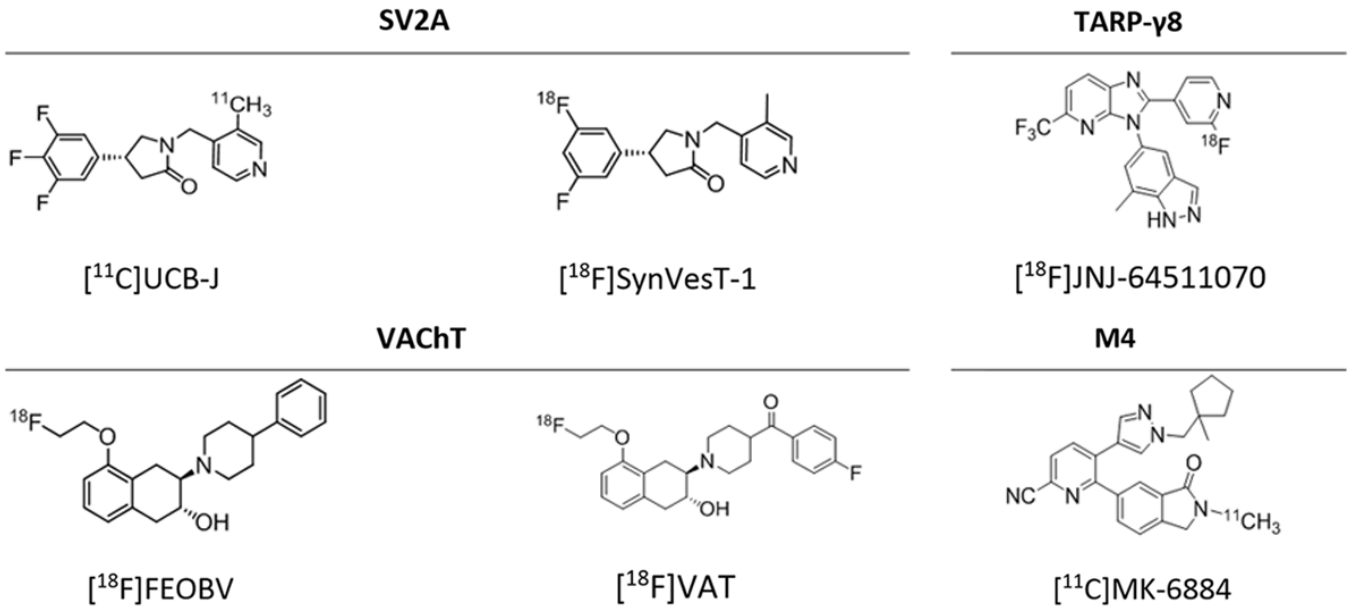

Figure 1. PET radiotracers and respective targets for clinical research interest in the present study.

ceuticals are (-)-5-[^{18}F]fluoroethoxybenzovesamicol ([^{18}F]FEOBV, **Figure 1**) which showed a decrease in tracer uptake in preclinical models with cholinergic deficit and in AD patients [22, 25-28] and [^{18}F]VAT (**Figure 1**), which is demonstrated to be a suitable PET radioligand for imaging VAChT *in vivo* [29-32] and has been recently translated to human studies (https://clinicaltrials.gov/study/NCT05034263).

The transmembrane α-amino-3-hydroxyl-5-methyl-4-isoxazole-propionic acid (AMPA) receptor regulatory protein γ8 (TARP-γ8) is a subunit of the AMPA receptors, ligand gated ion channels subgroup of the ionotropic glutamate receptors. TARP-γ8, predominantly found in the hippocampus, plays a crucial role in glutamatergic synaptic neurotransmission and plasticity, and has emerged as a promising target for PET [33-39]. Despite considerable efforts, the early generations of TARP-γ8 ligands suffered from poor CNS permeability, and high non-specific binding *in vivo* [40, 41]. Encouraging results were obtained for the TARP-γ8 candidates JNJ-55511118 [42] and LY-3130481, and the latter was advanced to Phase I clinical trials in 2017 [43-46]. More recently, the synthesis of selective TARP-γ8 ligands based on a benzothiazolone or an indazole scaffolds were reported and have high brain uptake and high specific binding to TARP-γ8 [47, 48]. [^{18}F]JNJ-64511070 (Scheme 1) is one of the promising candidate PET radiotracers, which exhibits desirable characteristics for the quantification of TARP-γ8 in the brain [49].

Muscarinic acetylcholine receptors (mAChRs) play a crucial role in the cholinergic pathway in mediating the actions of ACh [50]. Targeting mAChRs has demonstrated potential in the treatment of CNS disorders by alleviating psychosis and behavioral disorders [51]. Albeit, with five distinct mAChRs subtypes (M1-M5), ligand selectivity is crucial to ensure success in further clinical development [50]. The mAChR M4 subtype is expressed in key brain regions such as the striatum, hippocampus, and cortex [50]. Previous studies on this M4 subtype have demonstrated changes in its expression in neurodegenerative diseases such as AD, making it a viable target for disease diagnosis [50, 52]. The PET ligand [^{11}C]MK-6884 has shown selectivity for mAChR M4 over the other subtypes and a high brain uptake [53]. Recent clinical research in AD patients revealed the ability of [^{11}C]MK-6884 to show changes in mAChR M4 density and may provide crucial insights into neurodegenerative diseases diagnosis [54].

The objectives of this *in vitro* autoradiography (ARG) [55] study are: *i)* to compare the binding properties of two SV2A selective PET tracers, UCB-J and SynVesT-1, in post-mortem human brain tissues and quantify the reduction of synaptic density in AD cases; *ii)* to compare FEOBV and VAT for assessment of VAChT expression and presynaptic density in AD diagnosis; *iii)* to characterize JNJ-64511070 as a PET ligand for the quantification of TARP-γ8 in AD brains; *iv)* to determine the specific distribution of muscarinic M4 receptors *via* MK-6884 binding in AD tissues. To achieve these objectives, thin-section ARG binding assays were performed to compare the regional distribution of [^{3}H]UCB-J, [^{3}H]SynVesT-1, [^{18}F]FEOBV, [^{3}H]VAT, and [^{3}H]JNJ-64511070 in post-mortem tissue from five AD cases, three mild cognitive impairment (MCI) cases and three normal healthy volunteer (NHV) subjects in the cerebellum (CRB), the prefrontal cortex (PFC) and the hippocampus (HIP).

Results

Post-mortem healthy rodent (Figure S1) and human brain tissues were used to establish the distribution of the binding of all ligands in MCI and AD cases. Information

Table 1. Summary of the demographic data for the post-mortem brain samples used in the experiments

Conditions	Age (years)	Brain regions
AD	96	CRB, PFC
	67	CRB, PFC, HIP
	86	CRB, PFC
	88	HIP
	90	HIP
Average	85.4	-
MCI	86	CRB, PFC, HIP
	102	CRB, PFC, HIP
	79	CRB, PFC, HIP
Average	89	-
NHV	85	CRB, PFC, HIP
	72	CRB, PFC, HIP
	100	CRB, PFC
Average	85.67	-

regarding the gender and age of the subjects, as well as brain regions provided are summarized in **Table 1**. For this ARG binding study, the ^{18}F-labeled FEOBV was synthesized, and the four other radiotracers were obtained as tritium-labeled ligands.

Synaptic density

We evaluated the two tritium-labeled PET tracers, [^{3}H]UCB-J and [^{3}H]SynVesT-1, targeting SV2A in the three brain regions: HIP, PFC and CRB. Thin-section ARG was performed to evaluate the specific signal of the radiotracers to determine whether the radioligands provide a signal-to-noise ratio optimal for showing changes in radioligand binding between NHV, MCI and AD tissues (**Figure 2**). Both radiotracers displayed high specific binding when displaced using levetiracetam (200 µM), a known ligand for the SV2A receptor [56] in NHV (93.64 ± 1.94%, *n* = 2 for [^{3}H]UCB-J and 89.35 ± 2.50%, *n* = 2 for [^{3}H]SynVesT-1), MCI (93.41 ± 2.51%, *n* = 3 for [^{3}H]UCB-J and 90.18 ± 8.26%, *n* = 3 for [^{3}H]SynVesT-1) and AD (93.85 ± 2.55%, *n* = 3 for [^{3}H]UCB-J and 86.71 ± 10.49%, *n* = 3 for [^{3}H]SynVesT-1) tissues (**Figures 2**, S2, S6 and S10).

At equal ligand concentration, [^{3}H]UCB-J displayed a higher binding compared to [^{3}H]SynVesT-1 in AD, MCI and NHV tissues (**Figure 2**, in NHV (*n* = 2, dark blue), specific binding for [^{3}H]UCB-J: 145.56 ± 18.71 µCi/g *versus* 45.99 ± 5.72 µCi/g for [^{3}H]SynVesT-1). The ROI analysis showed a decrease in signal generated in MCI and AD tissues compared with NHV tissue sections for both [^{3}H]UCB-J and [^{3}H]SynVesT-1 in HIP. A depletion of 11% and 17% was observed in MCI and AD sections respectively for [^{3}H]UCB-J (**Figure 2**, specific binding: 145.56 ± 18.71 µCi/g in NHV tissues (*n* = 2, dark blue), 129.51 ± 35.17 µCi/g in MCI samples (*n* = 3, light blue) and 120.49 ± 16.40 µCi/g in AD cases (*n* = 3, orange)). The decrease was 5% and 37% in the same tissues for [^{3}H]SynVesT-1 (**Figure 2**, specific binding mean: 45.99 ± 5.72 µCi/g in NHV tissues (*n* = 3, dark blue), 43.59 ± 10.71 µCi/g in MCI samples (*n* = 3, light blue) and 29.12 ± 12.62 µCi/g in AD cases (*n* = 3, orange)).

VAChT

We evaluated [^{18}F]FEOBV and [^{3}H]VAT which both target VAChT, in the HIP, PFC and CRB (**Figures 3**, S3, S7 and S11). With previously reported conditions for the *in vitro* autoradiography binding techniques [26, 32], [^{18}F]FEOBV at 0.1 nM and [^{3}H]VAT at 10 nM displayed higher binding in all investigated gray matter regions than in the white matter. In NHV tissues, the binding for [^{18}F]FEOBV reached 0.65 ± 0.02 µCi/g in the PFC (*n* = 3), 0.73 ± 0.03 µCi/g in the CRB (*n* = 3) and was highest in the HIP at 1.26 ± 0.49 µCi/g (*n* = 2) (**Figure 3**). Similarly for [^{3}H]VAT in NHV tissues, the highest binding was found in the HIP at 16.27 ± 2.16 µCi/g (*n* = 2) and reached 6.59 ± 0.36 µCi/g in the PFC (*n* = 3) and 4.53 ± 0.56 µCi/g in the CRB (*n* = 3). Additionally, high specific binding was observed for [^{18}F]FEOBV and [^{3}H]VAT towards VAChT in the HIP (84.28 ± 3.25% for [^{18}F]FEOBV and 74.08 ± 7.29% for [^{3}H]VAT), the PFC (57.93 ± 10.25% for [^{18}F]FEOBV and 45.92 ± 6.36% for [^{3}H]VAT) and the CRB (63.56 ± 2.79% for [^{18}F]FEOBV and 42.29 ± 5.69% for [^{3}H]VAT). In the sample size used for this study (*n* = 3), no significant reductions in binding were observed for either [^{18}F]FEOBV nor for [^{3}H]VAT, in the MCI or AD cases in comparison to the NHV cases.

TARP-γ8

To characterize [^{3}H]JNJ-64511070 distribution in AD, MCI and NHV tissues, ARG was performed at a 2.5 nM radioligand concentration. The binding of [^{3}H]JNJ-64511070 was evaluated in the same sample cases as previously described. To the best of our knowledge, this is the first report of the binding of this tracer using *in vitro* thin section ARG. High specific binding was observed for [^{3}H]JNJ-64511070 towards TARP-γ8 in the presence of 10 µM of JNJ-64511070 in the HIP (92.32 ± 2.94%), PFC (67.88 ± 4.60%) and CRB (35.75 ± 11.04%) tissues (**Figures 4**, S4, S8 and S12).

When quantifying the binding, the TARP-γ8 compound revealed the lowest brain binding in AD and MCI brain tissues compared to NHV and showed 41% and 56% losses in the hippocampus in MCI and AD tissues, respectively (**Figure 4**, HIP, specific binding: 98.83 ± 46.25 µCi/g in NHV tissues (*n* = 2, dark blue), 58.56 ± 19.75 µCi/g in MCI samples (*n* = 3, light blue) and 43.27 ± 4.69 µCi/g in AD cases (*n* = 3, orange)). Binding in MCI and AD PFC sections was also found to be lower than in NHV tissues with a decrease of 8% and 15%, respectively (**Figure 4**, PFC, specific binding: 18.90 ± 0.44 µCi/g in NHV tissues (*n* = 3, dark blue), 17.30 ± 2.22 µCi/g in MCI samples (*n* = 3, light blue) and 16.10 ± 2.31 µCi/g in AD cases (*n* = 3, orange)).

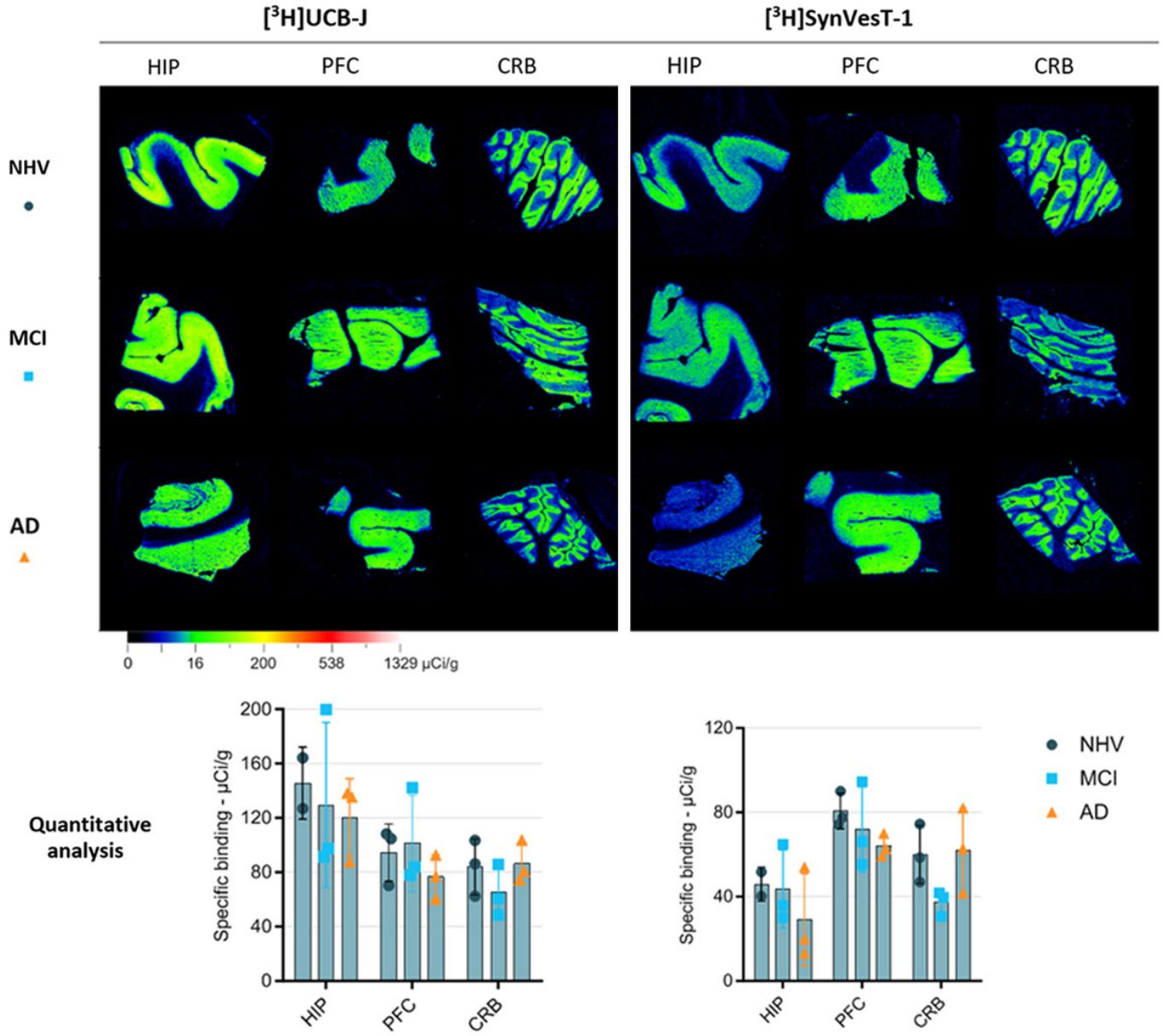

Figure 2. Representative autoradiograms of SV2A total binding sites in the HIP, PFC and CRB of NHV, MCI and AD patients for [^{3}H]UCB-J (left) and [^{3}H]SynVesT-1 (right); Quantification of the ARG signal in HIP, PFC, and CRB, for [^{3}H]UCB-J and [^{3}H]SynVesT-1 in NHV (dark blue), MCI (light blue) and AD (orange) post-mortem human brain sections. These slides were exposed to a phosphor sensor sheet for 4 days for [^{3}H]UCB-J and [^{3}H]SynVesT-1, and then scanned for visualizing and quantifying the ARG signal.

mAChR M4 subtype

The [^{3}H]MK-6884 distribution in MCI and AD tissues was demonstrated by ARG at 2.5 nM radioligand concentration in the presence of the cholinergic agonist carbachol (10 µM). Carbachol is a cholinergic agonist like acetylcholine activating muscarinic receptors increasing the affinity of [^{3}H]MK-6884 for the mAChR M4 subtype [53]. Due to a low overall binding, a moderate specific binding was observed for [^{3}H]MK-6884 towards M4 in the presence of 10 µM of MK-6884 in the hippocampus (59.48 ± 9.25%), PFC (60.60 ± 4.16%) and CRB (21.31 ± 4.31%) tissues (**Figures 5**, S5, S9 and S13). Nevertheless, a decrease in binding of 27% and 41%, respectively, was observed in MCI and AD tissues compared to NHV tissues in the hippocampus region (**Figure 5**, HIP, specific binding: 4.31 ± 0.83 µCi/g in NHV tissues (n = 2, dark blue), 3.15 ± 0.39 µCi/g in MCI samples (n = 3, light blue) and 2.55 ± 0.53 µCi/g in AD cases (n = 3, orange)).

Discussion

Changes in synaptic integrity in the hippocampus and prefrontal cortex is considered to be an important hallmark of AD [1]. This translates to the downregulation of several synaptic proteins [1]. In previous studies, [^{11}C]UCB-J detected reduced synaptic density in living patients with AD and MCI with an uptake reduction of 41% compared to NHV [57], while [^{18}F]SynVesT-1 was shown to have high brain uptake and high specific binding comparable to UCB-J [58]. [^{3}H]UCB-J and [^{3}H]SynVesT-1 were evaluated in NHV, MCI and tissues in our *in vitro* ARG

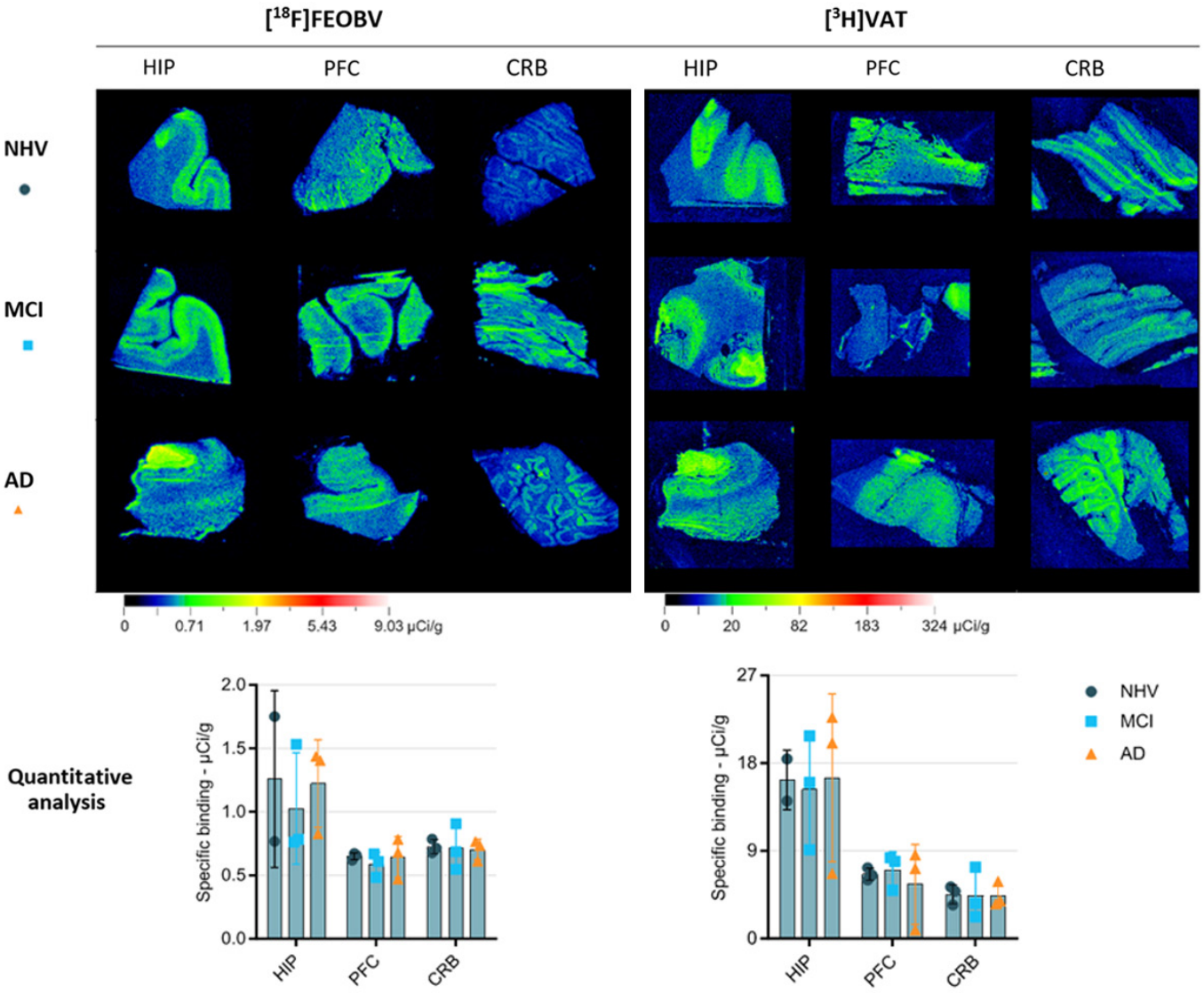

Figure 3. Representative autoradiograms of VAChT total binding sites in the HIP, PFC and CRB of NHV, MCI and AD patients for [^{18}F]FEOBV (left) and [^{3}H]VAT (right); Quantitative analysis of specific binding (µCi/g) in HIP, PFC, and CRB for [^{18}F]FEOBV (left) and [^{3}H]VAT (right), in NHV (dark blue), MCI (light blue) and AD (orange) human post-mortem brain sections. These slides were exposed to a phosphor sensor sheet for 20 min for [^{18}F]FEOBV or 14 days for [^{3}H]VAT, and then scanned for visualizing and quantifying the ARG signal.

study. All tissues showed reduction in binding for both tracers, with the greatest reduction in AD tissues for [^{3}H]SynVesT-1 (-37%) in comparison to [^{3}H]UCB-J (-17%). These results support previous ARG studies with [^{3}H]UCB-J including by Patel *et al.* who reported a reduction in cortex and hippocampus [61] as well as Mikkelsen *et al.* [62] who showed an 11% decrease in PFC. Our work is also consistent with the high specific binding shown by Kumar *et al.* [63], but contrasts with their data and work by Metaxas *et al.* [64] which did not find decreased binding of [^{3}H]UCB-J, albeit different experimental conditions need to be considered (large *vs.* small brain sections, different blocking agents and/or concentrations, etc.). Our study reinforces the important role of [^{18}F]SynVesT-1 for synaptic density evaluation in the living brain with applications in AD. [^{18}F]SynVesT-1 also offers the advantage of a ^{18}F-labeled tracer, and facilitates longer scanning protocols and multi-center clinical trials, and is being evaluated for human PET imaging studies at several laboratories, including ours [59, 60].

[^{18}F]FEOBV and [^{18}F]VAT are two promising VAChT-specific radiotracers with potential for imaging AD. As VAChT expression is considered to correlate with neurodegenerative disease progression, PET imaging with a suitable ligand would be a useful tool to assess the loss of cholinergic neurons in living subjects. Another goal of this study was to directly compare the binding ability of both [^{18}F]FEOBV and [^{3}H]VAT in the same tissue samples using *in vitro* ARG, to guide our clinical translation studies. ARG with [^{18}F]FEOBV has previously demonstrated a decrease in binding of 33% in the PFC (11 AD, 13 NHV) and 20% to 25% in hippocampus regions (8 AD, 13 NHV) in AD subjects compared to healthy tissues [65]. However, it is important to note the 20% to 40% overlap between AD

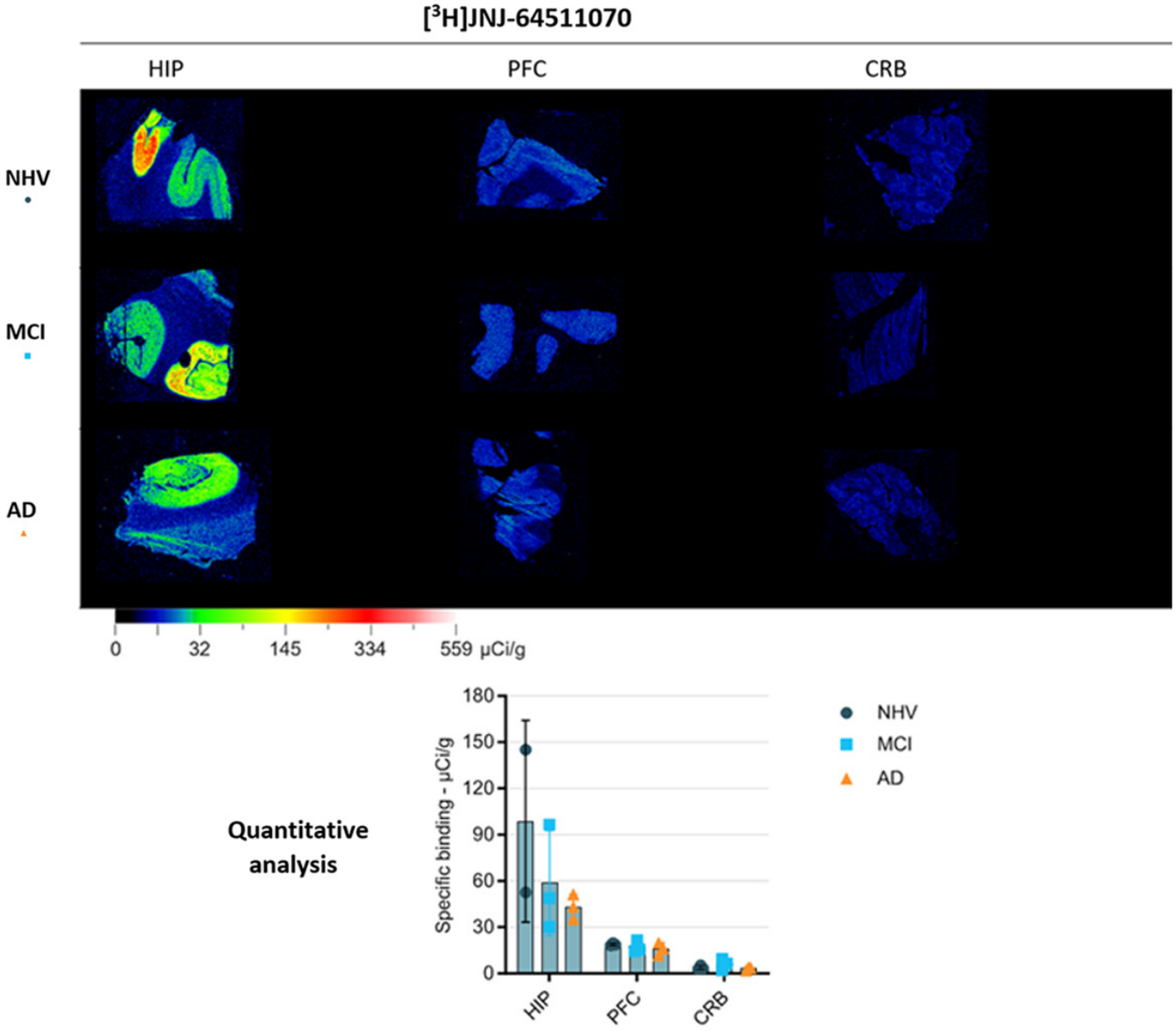

Figure 4. Representative autoradiograms of TARP-γ8 total binding sites in the HIP, PFC and CRB of NHV, MCI and AD patients; Quantification of the ARG signal for [^{3}H]JNJ-64511070 in the HIP, PFC, and CRB, in NHV (dark blue), MCI (light blue) and AD (orange) post-mortem human brain sections. These slides were exposed to a phosphor sensor sheet for 5 days for [^{3}H]JNJ-64511070, and then scanned for visualizing and quantifying the ARG signal.

and NHV tissues values. As some AD hallmarks have also been shown to correlate with ageing in rodents, including the synaptic dysfunction and changes in cholinergic neurons [66, 67], binding variation within the same group is variable as expected. This data is consistent with the present study, as we also observed an overlap between AD and NHV values for both [^{18}F]FEOBV and [^{3}H]VAT tracer binding levels between AD, MCI, and NHV brain sections. However, in our limited sample, these tracers were not sufficiently sensitive to differentiate AD from NHV.

Using the same human tissues, we evaluated the binding ability of [^{3}H]JNJ-64511070 in showing changes in TARP-γ8 expression between AD, MCI and NHV. To our knowledge, this is the first study investigating the binding of this tracer using ARG. [^{3}H]JNJ-64511070 was demonstrated to target TARP-γ8 with high specificity, with the highest binding in the hippocampal region. In our sample selection, the decrease in binding of [^{3}H]JNJ-64511070 in NHV, MCI and AD tissues was consistent with the degeneration in the glutamatergic pathway expected in AD pathologies. This approach may provide a direct assessment of TARP-γ8 expression in neurodegenerative diseases, our *in vitro* data supports the use of [^{18}F]JNJ-64511070 a promising radiotracer for AD diagnosis *in vivo*.

[^{11}C]MK-6884, a promising radiotracer targeting the mAChR M4 subtype, was evaluated in the same AD, MCI and NHV samples. Selectivity for M4 was shown as the tracer was displaced in the presence of MK-6884. A decrease in muscarinic M4 receptor density was observed

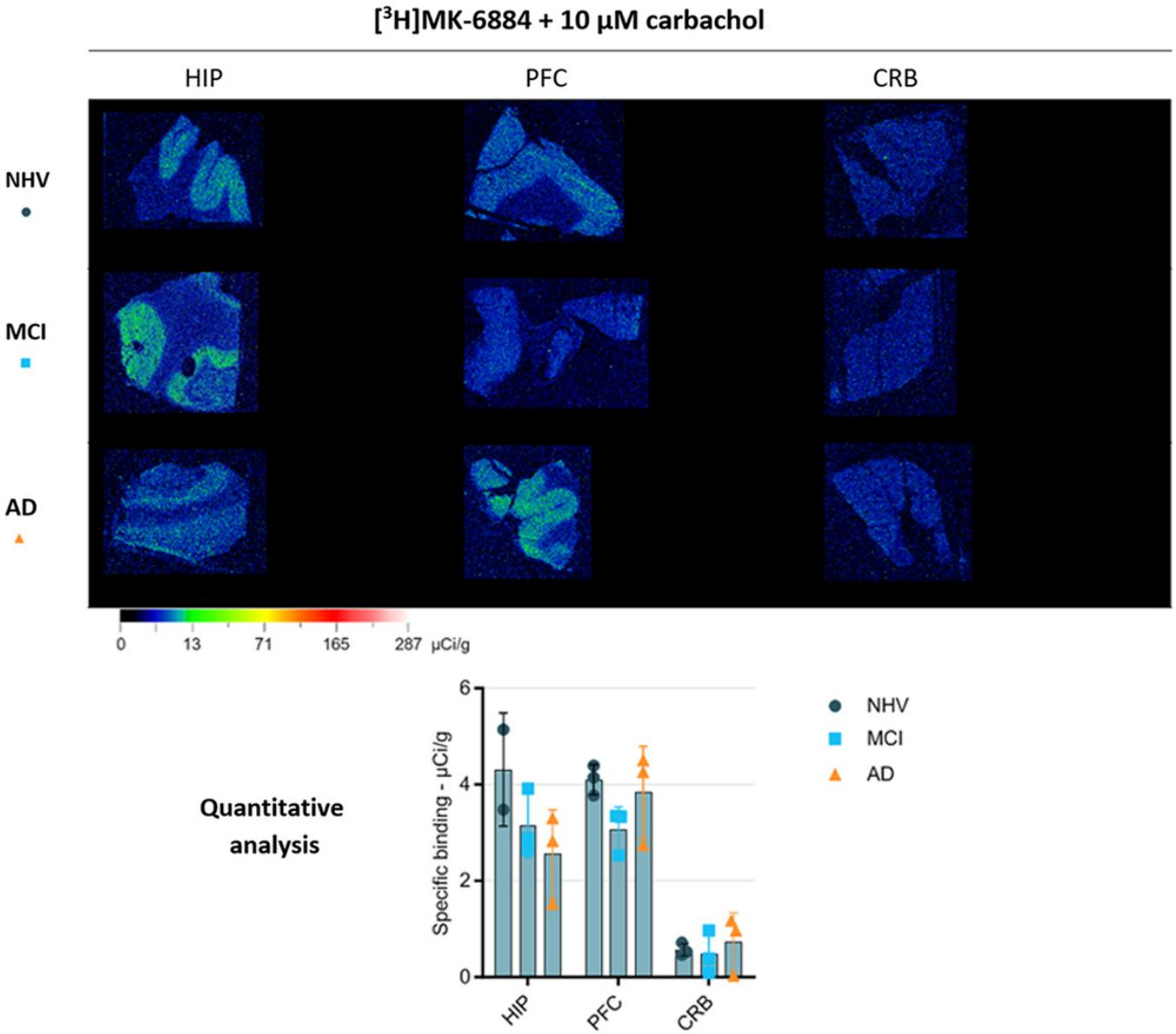

Figure 5. Representative autoradiograms of M4 total binding sites in the HIP, PFC and CRB of NHV, MCI and AD patients; Quantification of the ARG signal for [^{3}H]MK-6884 in HIP, PFC and CRB, in NHV (dark blue), MCI (light blue) and AD (orange) post-mortem human brain sections. These slides were exposed to a phosphor sensor sheet for 5 days for [^{3}H]MK-6884, and then scanned for visualizing and quantifying the ARG signal.

with [^{3}H]MK-6884 in human AD and MCI hippocampus tissues compared to NHV. These results confirmed the previous study obtained *in vivo* in patients with AD by Li *et al.* [54], in which an average decrease of 20% was obtained in individuals with AD compared to healthy adults. These data reveal the potential of [^{11}C]MK-6884 in providing crucial insights into neurodegenerative diseases diagnosis.

Limitations of the present study include tissue availability; a larger sample size would allow further interpretation of the radiotracers binding to AD pathology, as this work reveals variability in binding of several radiotracers between NHV, MCI and AD tissues. It would also be of value to evaluate sex differences and additional brain regions for analysis in future studies to explore PET tracer binding beyond the hippocampus, prefrontal cortex, and cerebellum in AD, for a greater representation of whole-brain imaging achieved with *in vivo* PET imaging studies.

Conclusions

Our preliminary work reveals that [^{3}H]UCB-J, [^{3}H]SynVesT-1, [^{3}H]JNJ-64511070, and [^{3}H]MK-6884, showed a decrease in their respective target density in human AD hippocampus tissues compared to NHV. This work will be used to guide our clinical research PET imaging programs and will continue to explore synaptic density *via* SV2A, TARP-γ8 and the mAChR M4 subtype for imaging in AD and related dementias.

Materials and methods

(2R,3R)-5-(2-tosyloxyethoxy)benzovesamicol and (2R,3R)-5-fluoroethoxy-benzovesamicol were provided by Eisai Inc (Nutley, NJ, USA). The reference compounds and associated tritiated radioligand [^{3}H]VAT (49 Ci/mmol), [^{3}H]JNJ-64511070 (34 Ci/mmol), [^{3}H]UCB-J (79 Ci/mmol) were provided by Enigma Biomedical Group (Boston, USA), MedChem Imaging (Boston, USA) and/or Novandi Chemistry AB (Södertälje, Sweden), and [^{3}H]SynVesT-1 (93 Ci/mmol) was purchased from Pharmaron (Cardiff, UK). TARP-γ8 antibody was purchased from Synaptic Systems (Goettingen, Germany).

[^{18}F]FEOBV was synthesized based on a method described previously [68, 69], with minor modifications. Briefly, reaction of the tosyloxy precursor, (2R,3R)-5-(2-tosyloxyethoxy) benzovesamicol, with [^{18}F]fluoride ion in dimethylsulfoxide followed by purification using preparative high-pressure liquid chromatography (45% MeCN:55% aq. 50 mM ammonium acetate, 6 mL/min, t_R = 23 min) provided the desired [^{18}F]FEOBV with a decay-corrected radiochemical yield of 8 ± 2% (*n* = 5), a high radiochemical purity (>99%) and a molar activity of 209 ± 66 GBq/μmol at the end of synthesis. The synthesis was fully automated using a GE TRACERlab FX_{FN} synthesis module, and the synthesis time was 60 ± 5 min from the end of bombardment.

In vitro autoradiography

Frozen brain samples from NHV, MCI and AD-positive brains were obtained from Eisai Inc. or in-house, in accordance with the guidelines put forth by the Centre for Addiction and Mental Health Research Ethics Board (protocol 036-2019). In total, 26 samples from 11 individuals between 67 and 102 years old were provided: 8 samples from the hippocampus (2 NHV, 3 MCI, 3 AD), 9 from the prefrontal cortex (PFC) (3 NHV, 3 MCI, 3 AD) and 9 from the cerebellum (3 NHV, 3 MCI, 3 AD). Using a freezing sliding microtome (CryoStar NX50) at -16°C, each block of tissue was cut into serial 10 μm-thick sections, which were then thaw-mounted on coated microscope slides (Fisher Superfrost Plus Gold) and stored at -80°C for later use.

The optimal conditions for the *in vitro* ARG binding techniques such as incubation time, washing procedure, and time of exposition to the phosphor imaging plate were obtained after preliminary experiments on rodent brain. The sections were then exposed on a radioluminographic imaging plate (Fujifilm BAS-TR2040, GE Healthcare) for the indicated time. The autoradiography signal was visualized on an Amersham Typhoon phosphorimager (GE Healthcare, USA). The radioactivity was quantified using MCID 7.0 imaging suite (Interfocus Imaging, Cambridge, UK) by drawing regions of interest (ROIs). The binding was expressed in μCi/g for [^{18}F]FEOBV and for the ^{3}H-labeled tracers, using commercial tritium standards (American Radiolabeled Chemicals Inc.; St. Louis, USA). Percent specific binding (% Specific binding = ((Total signal - Non-specific signal)/(Total signal)) *100) is reported.

[^{3}H]UCB-J, procedure adapted from Patel et al. [61]: Brain sections were warmed up to room temperature, and pre-incubated in the binding buffer (50 mM Tris-HCl buffer containing 140 mM NaCl, 5 mM KCl, 1.5 mM $MgCl_2.6H_2O$ and 1.5 mM $CaCl_2.H_2O$ at pH 7.4) for 15 min. Tissues were incubated with 2 nM of [^{3}H]UCBJ (for total binding), or with the addition of 200 μM of levetiracetam as a blocking agent (for non-specific binding) for 1 h at room temperature. After incubation, the slides were washed twice for 1 min in ice-cold binding buffer, rinsed in ice-cold distilled water, air-dried, and exposed for 4 days.

[^{3}H]SynVesT-1, procedure adapted from Patel et al. [61]: Brain sections were warmed up to room temperature, and preincubated in the binding buffer (50 mM Tris-HCl buffer containing 140 mM NaCl, 5 mM KCl, 1.5 mM $MgCl_2.6H_2O$ and 1.5 mM $CaCl_2.H_2O$ at pH 7.4) for 15 min. Tissues were incubated with 2 nM of [^{3}H]SynVesT-1 (for total binding), or with the addition of 200 μM of levetiracetam as a blocking agent (for non-specific binding) for 1 h at room temperature. After incubation, the slides were washed twice for 1 min in ice-cold binding buffer, rinsed in ice-cold distilled water, air-dried, and exposed for 4 days.

[^{18}F]FEOBV, procedure adapted from Parent et al. [65]: Brain sections were warmed up to room temperature, and preincubated in a phosphate-buffered saline solution for 20 min. Tissues were then incubated with 0.1 nM of [^{18}F]FEOBV (for total binding), or with addition of 10 μM of cold self as a blocking agent (for non-specific binding), in the same buffer solution for 20 min at room temperature. After incubation, the slides were rinsed in ice-cold distilled water, air-dried, and exposed for 5 minutes.

[^{3}H]VAT, procedure adapted from Liang et al. [32]: Brain sections were warmed up to room temperature, and pre-incubated in the binding buffer (50 mM Tris-HCl buffer containing 1.2 mM NaCl and 1 mM EDTA at pH 7.4) for 20 min. Tissues were incubated with 10 nM of [^{3}H]VAT (for total binding), or with the addition of 10 μM of cold "self" as a blocking agent (for non-specific binding) for 1 h at room temperature. After incubation, the slides were washed twice for 4 min in ice-cold binding buffer, rinsed in ice-cold distilled water, air-dried, and exposed for 8 days.

[^{3}H]JNJ-64511070, procedure adapted from Chen et al. [40]: Brain sections were warmed up to room temperature, and preincubated in a phosphate-buffered saline solution for 20 min. Tissues were incubated with 2.5 nM of [^{3}H]JNJ-64511070 (for total binding) in the binding buffer (50 mM Tris-HCl buffer containing 1.2 mM NaCl and 2 mM $MgCl_2.6H_2O$ at pH 7.4), or with the addition of 10 μM of cold "self" as a blocking agent (for non-specific binding) for 1 h at room temperature. After incubation, the slides

were washed 3 times for 2 min in ice-cold binding buffer, rinsed in ice-cold distilled water, air-dried, and exposed for 5 days.

[^{3}H]MK-6884: Brain sections were warmed up to room temperature, and preincubated in the binding buffer (50 mM Tris-HCl buffer containing 1.2 mM NaCl, 2 mM KCl, 2 mM $MgCl_2.6H_2O$ and 1 mM $CaCl_2$ at pH 7.4) for 20 min. Tissues were incubated with 2.5 nM of [^{3}H]MK-6884 (for total binding), or with the addition of 10 μM of cold self as a blocking agent (for non-specific binding) for 1 h at room temperature. After incubation, the slides were washed twice for 4 min in ice-cold binding buffer, rinsed in ice-cold distilled water, air-dried, and exposed for 5 days.

Acknowledgements

We thank the staff in the Azrieli Centre for Neuro-Radiochemistry at CAMH for their support with the radiochemistry experiments. We also thank Dr. Cassis Varlow for reviewing the manuscript and colleagues from Eisai Inc. for helpful discussions. And we thank Enigma Biomedical Group, Inc. for providing reference standards and radiotracers as well as for support, as well as Eisai Inc. for support. F.d'O. thanks the Swiss National Foundation for supporting. N.V. thanks the Azrieli Foundation, the Canada Research Chairs Program, Canada Foundation for Innovation, and the Ontario Research Fund.

Disclosure of conflict of interest

N.V. is a co-founder of MedChem Imaging, Inc., S.K. was an employee of Eisai Inc. when the work was undertaken, and A.C. and P.S. are currently employees of Eisai Inc.

Address correspondence to: Neil Vasdev, Azrieli Centre for Neuro-Radiochemistry, Brain Health Imaging Centre, Centre for Addiction and Mental Health (CAMH), Toronto, ON, Canada. E-mail: neil.vasdev@utoronto.ca

References

[1] Honer WG. Pathology of presynaptic proteins in Alzheimer's disease: More than simple loss of terminals. Neurobiol Aging 2003; 24: 1047-62.

[2] Robinson JL, Molina-Porcel L, Corrada MM, Raible K, Lee EB, Lee VM, Kawas CH and Trojanowski JQ. Perforant path synaptic loss correlates with cognitive impairment and Alzheimer's disease in the oldest-old. Brain 2014; 137: 2578-87.

[3] Bao W, Jia H, Finnema S, Cai Z, Carson RE and Huang YH. PET imaging for early detection of Alzheimer's disease: from pathologic to physiologic biomarkers. PET Clin 2017; 12: 329-50.

[4] Cai Z, Li S, Matuskey D, Nabulsi N and Huang Y. PET imaging of synaptic density: a new tool for investigation of neuropsychiatric diseases. Neurosci Lett 2019; 691: 44-50.

[5] Nabulsi NB, Mercier J, Holden D, Carré S, Najafzadeh S, Vandergeten MC, Lin SF, Deo A, Price N, Wood M, Lara-Jaime T, Montel F, Laruelle M, Carson RE, Hannestad J and Huang Y. Synthesis and preclinical evaluation of 11C-UCB-J as a PET tracer for imaging the synaptic vesicle glycoprotein 2A in the brain. J Nucl Med 2016; 57: 777-84.

[6] Finnema SJ, Nabulsi NB, Eid T, Detyniecki K, Lin SF, Chen MK, Dhaher R, Matuskey D, Baum E, Holden D, Spencer DD, Mercier J, Hannestad J, Huang Y and Carson RE. Imaging synaptic density in the living human brain. Sci Transl Med 2016; 8: 348ra96.

[7] Finnema SJ, Nabulsi NB, Mercier J, Lin SF, Chen MK, Matuskey D, Gallezot JD, Henry S, Hannestad J, Huang Y and Carson RE. Kinetic evaluation and test-retest reproducibility of [11C]UCB-J, a novel radioligand for positron emission tomography imaging of synaptic vesicle glycoprotein 2A in humans. J Cereb Blood Flow Metab 2018; 38: 2041-52.

[8] Li S, Cai Z, Wu X, Holden D, Pracitto R, Kapinos M, Gao H, Labaree D, Nabulsi N, Carson RE and Huang Y. Synthesis and in vivo evaluation of a novel PET radiotracer for imaging of synaptic vesicle glycoprotein 2A (SV2A) in nonhuman primates. ACS Chem Neurosci 2019; 10: 1544-54.

[9] Constantinescu CC, Tresse C, Zheng M, Gouasmat A, Carroll VM, Mistico L, Alagille D, Sandiego CM, Papin C, Marek K, Seibyl JP, Tamagnan GD and Barret O. Development and in vivo preclinical imaging of fluorine-18-labeled synaptic vesicle protein 2A (SV2A) PET tracers. Mol Imaging Biol 2019; 21: 509-18.

[10] Arvidsson U, Riedl M, Elde R and Meister B. Vesicular acetylcholine transporter (VAChT) protein: a novel and unique marker for cholinergic neurons in the central and peripheral nervous systems. J Comp Neurol 1997; 378: 454-67.

[11] Whitehouse PJ, Price DL, Struble RG, Clark AW, Coyle JT and Delon MR. Alzheimer's disease and senile dementia: loss of neurons in the basal forebrain. Science 1982; 215: 1237-9.

[12] Coyle JT, Price DL and Delong MR. Alzheimer's disease: a disorder of cortical cholinergic innervation. Science 1983; 219: 1184-90.

[13] Hilker R, Thomas AV, Klein JC, Weisenbach S, Kalbe E, Burghaus L, Jacobs AH, Herholz K and Heiss WD. Dementia in Parkinson disease: functional imaging of cholinergic and dopaminergic pathways. Neurology 2005; 65: 1716-22.

[14] Armstrong RA. What causes Alzheimer's disease? Folia Neuropathol 2013; 51: 169-88.

[15] Prado VF, Roy A, Kolisnyk B, Gros R and Prado MA. Regulation of cholinergic activity by the vesicular acetylcholine transporter. Biochem J 2013; 450: 265-74.

[16] Schliebs R and Arendt T. The significance of the cholinergic system in the brain during aging and in Alzheimer's disease. J Neural Transm (Vienna) 2006; 113: 1625-44.

[17] Schliebs R and Arendt T. The cholinergic system in aging and neuronal degeneration. Behav Brain Res 2011; 221: 555-63.

[18] Giboureau N, Aumann KM, Beinat C and Kassiou M. Development of vesicular acetylcholine transporter ligands: molecular probes for Alzheimer's disease. Curr Bioact Compd 2010; 6: 129-55.

[19] Giboureau N, Som IM, Boucher-Arnold A, Guilloteau D and Kassiou M. PET radioligands for the vesicular acetylcholine transporter (VAChT). Curr Top Med Chem 2010; 10: 1569-83.

[20] Efange SM, Khare AB, Von Hohenberg K, MacH RH, Parsons SM and Tu Z. Synthesis and in vitro biological evaluation of carbonyl group-containing inhibitors of ve-

sicular acetylcholine transporter. J Med Chem 2010; 53: 2825-35.
[21] Petrou M, Frey KA, Kilbourn MR, Scott PJ, Raffel DM, Bohnen NI, Müller ML, Albin RL and Koeppe RA. In vivo imaging of human cholinergic nerve terminals with (-)-5-18F-fluoroethoxybenzovesamicol: biodistribution, dosimetry, and tracer kinetic analyses. J Nucl Med 2014; 55: 396-404.
[22] Cyr M, Parent MJ, Mechawar N, Rosa-Neto P, Soucy JP, Aliaga A, Kostikov A, Maclaren DA, Clark SD and Bedard MA. PET imaging with [18F]fluoroethoxybenzovesamicol ([18F]FEOBV) following selective lesion of cholinergic pedunculopontine tegmental neurons in rat. Nucl Med Biol 2014; 41: 96-101.
[23] Giboureau N, Emond P, Fulton RR, Henderson DJ, Chalon S, Garreau L, Roselt P, Eberl S, Mavel S, Bodard S, Fulham MJ, Guilloteau D and Kassiou M. Ex vivo and in vivo evaluation of (2R,3R)-5-[18F]-fluoroethoxy- and fluoropropoxybenzovesamicol, as PET radioligands for the vesicular acetylcholine transporter. Synapse 2007; 61: 962-70.
[24] Barthel C, Sorger D, Deuther-Conrad W, Scheunemann M, Schweiger S, Jäckel P, Roghani A, Steinbach J, Schüürmann G, Sabri O, Brust P and Wenzel B. New systematically modified vesamicol analogs and their affinity and selectivity for the vesicular acetylcholine transporter - A critical examination of the lead structure. Eur J Med Chem 2015; 100: 50-67.
[25] Parent M, Bedard MA, Aliaga A, Soucy JP, Landry St-Pierre E, Cyr M, Kostikov A, Schirrmacher E, Massarweh G and Rosa-Neto P. PET imaging of cholinergic deficits in rats using [18F]fluoroethoxybenzovesamicol ([18F]FEOBV). Neuroimage 2012; 62: 555-61.
[26] Parent MJ, Cyr M, Aliaga A, Kostikov A, Schirrmacher E, Soucy JP, Mechawar N, Rosa-Neto P and Bedard MA. Concordance between in vivo and postmortem measurements of cholinergic denervation in rats using pet with [18F]FEOBV and choline acetyltransferase immunochemistry. EJNMMI Res 2013; 3: 70.
[27] Cyr M, Parent MJ, Mechawar N, Rosa-Neto P, Soucy JP, Clark SD, Aghourian M and Bedard MA. Deficit in sustained attention following selective cholinergic lesion of the pedunculopontine tegmental nucleus in rat, as measured with both post-mortem immunocytochemistry and in vivo PET imaging with [18F]fluoroethoxybenzovesamicol. Behav Brain Res 2015; 278: 107-14.
[28] Aghourian M, Legault-Denis C, Soucy JP, Rosa-Neto P, Gauthier S, Kostikov A, Gravel P and Bédard MA. Quantification of brain cholinergic denervation in Alzheimer's disease using PET imaging with [18F]-FEOBV. Mol Psychiatry 2017; 22: 1531-8.
[29] Tu Z, Zhang X, Jin H, Yue X, Padakanti PK, Yu L, Liu H, Flores HP, Kaneshige K, Parsons SM and Perlmutter JS. Synthesis and biological characterization of a promising F-18 PET tracer for vesicular acetylcholine transporter. Bioorg Med Chem 2015; 23: 4699-709.
[30] Karimi M, Tu Z, Yue X, Zhang X, Jin H, Perlmutter JS and Laforest R. Radiation dosimetry of [18F]VAT in nonhuman primates. EJNMMI Res 2015; 5: 73.
[31] Jin H, Yue X, Liu H, Han J, Flores H, Su Y, Parsons SM, Perlmutter JS and Tu Z. Kinetic modeling of [18F]VAT, a novel radioligand for positron emission tomography imaging vesicular acetylcholine transporter in non-human primate brain. J Neurochem 2018; 144: 791-804.
[32] Liang Q, Joshi S, Liu H, Yu Y, Zhao H, Benzinger TLS, Perlmutter JS and Tu Z. In vitro characterization of [3H]VAT in cells, animal and human brain tissues for vesicular acetylcholine transporter. Eur J Pharmacol 2021; 911: 174556.
[33] Hollmann M and Heinemann S. Cloned glutamate receptors. Annu Rev Neurosci 1994; 17: 31-108.
[34] Mayer ML and Armstrong N. Structure and function of glutamate receptor ion channels. Annu Rev Physiol 2004; 66: 161-81.
[35] Traynelis SF, Wollmuth LP, McBain CJ, Menniti FS, Vance KM, Ogden KK, Hansen KB, Yuan H, Myers SJ and Dingledine R. Glutamate receptor ion channels: structure, regulation, and function. Pharmacol Rev 2010; 62: 405-96.
[36] Tomita S, Chen L, Kawasaki Y, Petralia RS, Wenthold RJ, Nicoll RA and Bredt DS. Functional studies and distribution define a family of transmembrane AMPA receptor regulatory proteins. J Cell Biol 2003; 161: 805-16.
[37] Rouach N, Byrd K, Petralia RS, Elias GM, Adesnik H, Tomita S, Karimzadegan S, Kealey C, Bredt DS and Nicoll RA. TARP γ-8 controls hippocampal AMPA receptor number, distribution and synaptic plasticity. Nat Neurosci 2005; 8: 1525-33.
[38] Fukaya M, Tsujita M, Yamazaki M, Kushiya E, Abe M, Akashi K, Natsume R, Kano M, Kamiya H, Watanabe M and Sakimura K. Abundant distribution of TARP γ-8 in synaptic and extrasynaptic surface of hippocampal neurons and its major role in AMPA receptor expression on spines and dendrites. Eur J Neurosci 2006; 24: 2177-90.
[39] Yamasaki M, Fukaya M, Yamazaki M, Azechi H, Natsume R, Abe M, Sakimura K and Watanabe M. TARP γ-2 and γ-8 differentially control AMPAR density across schaffer collateral/commissural synapses in the hippocampal CA1 area. J Neurosci 2016; 36: 4296-312.
[40] Chen Z, Mori W, Zhang X, Yamasaki T, Dunn PJ, Zhang G, Fu H, Shao T, Zhang Y, Hatori A, Ma L, Fujinaga M, Xie L, Deng X, Li H, Yu Q, Rong J, Josephson L, Ma JA, Shao Y, Tomita S, Zhang MR and Liang SH. Synthesis, pharmacology and preclinical evaluation of 11C-labeled 1,3-dihydro-2H-benzo[d]imidazole-2-ones for imaging γ8-dependent transmembrane AMPA receptor regulatory protein. Eur J Med Chem 2018; 157: 898-908.
[41] Zwart R, Sher E, Ping X, Jin X, Sims JR Jr, Chappell AS, Gleason SD, Hahn PJ, Gardinier K, Gernert DL, Hobbs J, Smith JL, Valli SN and Witkin JM. Perampanel, an antagonist of a-amino-3-hydroxy-5-methyl-4-isoxazolepropionic acid receptors, for the treatment of epilepsy: studies in human epileptic brain and nonepileptic brain and in rodent models. J Pharmacol Exp Ther 2014; 351: 124-33.
[42] Maher MP, Wu N, Ravula S, Ameriks MK, Savall BM, Liu C, Lord B, Wyatt RM, Matta JA, Dugovic C, Yun S, Ver Donck L, Steckler T, Wickenden AD, Carruthers NI and Lovenberg TW. Discovery and characterization of AMPA receptor modulators selective for TARP-γ8. J Pharmacol Exp Ther 2016; 357: 394-414.
[43] Gardinier KM, Gernert DL, Porter WJ, Reel JK, Ornstein PL, Spinazze P, Stevens FC, Hahn P, Hollinshead SP, Mayhugh D, Schkeryantz J, Khilevich A, De Frutos O, Gleason SD, Kato AS, Luffer-Atlas D, Desai PV, Swanson S, Burris KD, Ding C, Heinz BA, Need AB, Barth VN, Stephenson GA, Diseroad BA, Woods TA, Yu H, Bredt D and Witkin JM. Discovery of the first α-amino-3-hydroxy-5-methyl-4-

isoxazolepropionic acid (AMPA) receptor antagonist dependent upon transmembrane AMPA receptor regulatory protein (TARP) γ-8. J Med Chem 2016; 59: 4753-68.
[44] Kato AS, Burris KD, Gardinier KM, Gernert DL, Porter WJ, Reel J, Ding C, Tu Y, Schober DA, Lee MR, Heinz BA, Fitch TE, Gleason SD, Catlow JT, Yu H, Fitzjohn SM, Pasqui F, Wang H, Qian Y, Sher E, Zwart R, Wafford KA, Rasmussen K, Ornstein PL, Isaac JT, Nisenbaum ES, Bredt DS and Witkin JM. Forebrain-selective AMPA-receptor antagonism guided by TARP γ-8 as an antiepileptic mechanism. Nat Med 2016; 22: 1496-501.
[45] Lee MR, Gardinier KM, Gernert DL, Schober DA, Wright RA, Wang H, Qian Y, Witkin JM, Nisenbaum ES and Kato AS. Structural determinants of the γ-8 TARP dependent AMPA receptor antagonist. ACS Chem Neurosci 2017; 8: 2631-47.
[46] Witkin JM, Li J, Gilmour G, Mitchell SN, Carter G, Gleason SD, Seidel WF, Eastwood BJ, McCarthy A, Porter WJ, Reel J, Gardinier KM, Kato AS and Wafford KA. Electroencephalographic, cognitive, and neurochemical effects of LY3130481 (CERC-611), a selective antagonist of TARP-γ8-associated AMPA receptors. Neuropharmacology 2017; 126: 257-70.
[47] Savall BM, Wu D, Swanson DM, Seierstad M, Wu N, Vives Martinez J, García Olmos B, Lord B, Coe K, Koudriakova T, Lovenberg TW, Carruthers NI, Maher MP and Ameriks MK. Discovery of imidazo[1,2-a]pyrazines and pyrazolo[1,5-c] pyrimidines as TARP γ-8 selective AMPAR negative modulators. ACS Med Chem Lett 2018; 10: 267-72.
[48] Yu Q, Kumata K, Rong J, Chen Z, Yamasaki T, Chen J, Xiao Z, Ishii H, Hiraishi A, Shao T, Zhang Y, Hu K, Xie L, Fujinaga M, Zhao C, Mori W, Collier T, Haider A, Tomita S, Zhang MR and Liang S. Imaging of transmembrane AMPA receptor regulatory proteins by positron emission tomography. J Med Chem 2022; 65: 9144-58.
[49] Berry CGB, Chen G, Jourdan FL, Lebold T, Lin DW, Pena Pinon MA, Ravula S, Savall BM, Swanson DM, Wu D, Zhang W and Ameriks MK. Azabenzimidazoles and their use as AMPA receptor modulators. 2016.
[50] Lebois EP, Thorn C, Edgerton JR, Popiolek M and Xi S. Muscarinic receptor subtype distribution in the central nervous system and relevance to aging and Alzheimer's disease. Neuropharmacology 2018; 136: 362-73.
[51] Conn PJ, Lindsley CW, Meiler J and Niswender CM. Opportunities and challenges in the discovery of allosteric modulators of GPCRs for treating CNS disorders. Nat Rev Drug Discov 2014; 13: 692-708.
[52] Scarr E, McLean C and Dean B. Higher levels of different muscarinic receptors in the cortex and hippocampus from subjects with Alzheimer's disease. J Neural Transm (Vienna) 2017; 124: 273-84.
[53] Tong L, Li W, Lo MM, Gao X, Wai JM, Rudd M, Tellers D, Joshi A, Zeng Z, Miller P, Salinas C, Riffel K, Haley H, Purcell M, Holahan M, Gantert L, Schubert JW, Jones K, Mulhearn J, Egbertson M, Meng Z, Hanney B, Gomez R, Harrison ST, McQuade P, Bueters T, Uslaner J, Morrow J, Thomson F, Kong J, Liao J, Selyutin O, Bao J, Hastings NB, Agrawal S, Magliaro BC, Monsma FJ Jr, Smith MD, Risso S, Hesk D, Hostetler E and Mazzola R. Discovery of [11C]MK-6884: a positron emission tomography (PET) imaging agent for the study of M4 muscarinic receptor positive allosteric modulators (PAMs) in neurodegenerative diseases. J Med Chem 2020; 63: 2411-25.
[54] Li W, Wang Y, Lohith TG, Zeng Z, Tong L, Mazzola R, Riffel K, Miller P, Purcell M, Holahan M, Haley H, Gantert L, Hesk D, Ren S, Morrow J, Uslaner J, Struyk A, Wai JM, Rudd MT, Tellers DM, McAvoy T, Bormans G, Koole M, Van Laere K, Serdons K, de Hoon J, Declercq R, De Lepeleire I, Pascual MB, Zanotti-Fregonara P, Yu M, Arbones V, Masdeu JC, Cheng A, Hussain A, Bueters T, Anderson MS, Hostetler ED and Basile AS. The PET tracer [11C]MK-6884 quantifies M4 muscarinic receptor in rhesus monkeys and patients with Alzheimer's disease. Sci Transl Med 2022; 14: eabg3684.
[55] Lever SZ, Fan KH and Lever JR. Tactics for preclinical validation of receptor-binding radiotracers. Nucl Med Biol 2017; 44: 4-30.
[56] Lynch BA, Lambeng N, Nocka K, Kensel-Hammes P, Bajjalieh SM, Matagne A and Fuks B. The synaptic vesicle protein SV2A is the binding site for the antiepileptic drug levetiracetam. Proc Natl Acad Sci U S A 2004; 101: 9861-6.
[57] Chen MK, Mecca AP, Naganawa M, Finnema SJ, Toyonaga T, Lin SF, Najafzadeh S, Ropchan J, Lu Y, McDonald JW, Michalak HR, Nabulsi NB, Arnsten AFT, Huang Y, Carson RE and van Dyck CH. Assessing synaptic density in Alzheimer disease with synaptic vesicle glycoprotein 2A positron emission tomographic imaging. JAMA Neurol 2018; 75: 1215-24.
[58] Naganawa M, Li S, Nabulsi N, Henry S, Zheng MQ, Pracitto R, Cai Z, Gao H, Kapinos M, Labaree D, Matuskey D, Huang Y and Carson RE. First-in-human evaluation of 18F-SynVesT-1, a radioligand for PET imaging of synaptic vesicle glycoprotein 2A. J Nucl Med 2021; 62: 561-7.
[59] Desmond KL, Lindberg A, Garcia A, Tong J, Harkness MB, Dobrota E, Smart K, Uribe C, Meyer JH, Houle S, Strafella AP, Li S, Huang Y and Vasdev N. First-in-human PET imaging of [18F]SDM-4MP3: a cautionary tale. Mol Imaging 2023; 2023: 8826977.
[60] Smart K, Uribe C, Desmond KL, Martin SL, Vasdev N and Strafella AP. Preliminary assessment of reference region quantification and reduced scanning times for [18F] SynVesT-1 PET in Parkinson's disease. Mol Imaging 2023; 2023: 1855985.
[61] Patel S, Knight A, Krause S, Teceno T, Tresse C, Li S, Cai Z, Gouasmat A, Carroll VM, Barret O, Gottmukkala V, Zhang W, Xiang X, Morley T, Huang Y and Passchier J. Preclinical in vitro and in vivo characterization of synaptic vesicle 2A-targeting compounds amenable to F-18 labeling as potential PET radioligands for imaging of synapse integrity. Mol Imaging Biol 2020; 22: 832-41.
[62] Mikkelsen JD, Kaad S, Aripaka SS and Finsen B. Synaptic vesicle glycoprotein 2A (SV2A) levels in the cerebral cortex in patients with Alzheimer's disease: a radioligand binding study in postmortem brains. Neurobiol Aging 2023; 129: 50-7.
[63] Kumar A, Scarpa M and Nordberg A. Tracing synaptic loss in Alzheimer's brain with SV2A PET-tracer UCB-J. Alzheimers Dement 2024; [Epub ahead of print].
[64] Metaxas A, Thygesen C, Briting SRR, Landau AM, Darvesh S and Finsen B. Increased inflammation and unchanged density of synaptic vesicle glycoprotein 2A (SV2A) in the postmortem frontal cortex of Alzheimer's disease patients. Front Cell Neurosci 2019; 13: 538.
[65] Parent MJ, Bedard MA, Aliaga A, Minuzzi L, Mechawar N, Soucy JP, Schirrmacher E, Kostikov A, Gauthier SG and

Rosa-Neto P. Cholinergic depletion in Alzheimer's disease shown by [18F]FEOBV autoradiography. Int J Mol Imaging 2013; 2013: 205045.

[66] Sherman KA and Friedman E. Pre- and post-synaptic cholinergic dysfunction in aged rodent brain regions: new findings and an interpretative review. Int J Dev Neurosci 1990; 8: 689-708.

[67] Canas PM, Duarte JM, Rodrigues RJ, Köfalvi A and Cunha RA. Modification upon aging of the density of presynaptic modulation systems in the hippocampus. Neurobiol Aging 2009; 30: 1877-84.

[68] Mulholland GK, Jung YW, Wieland DM, Kilboum MR and Kuhl DE. Synthesis of [18F]Fluoroethoxy-benzovesamicol, a radiotracer for cholinergic neurons. J Labelled Comp Radiopharm 1993; 33: 583-91.

[69] Hockley BG, Stewart MN and Scott PJH. Synthesis of [18F]-(-)Fluoroethoxy benzovesamicol ([18F]FEOBV). Radiochemical Syntheses, Volume 2: Further Radiopharmaceuticals for Positron Emission Tomography and New Strategies for Their Production, First Edition Edited of [18F]. 2015. pp. 13-20.

Distribution in sagittal sections of healthy rat brain

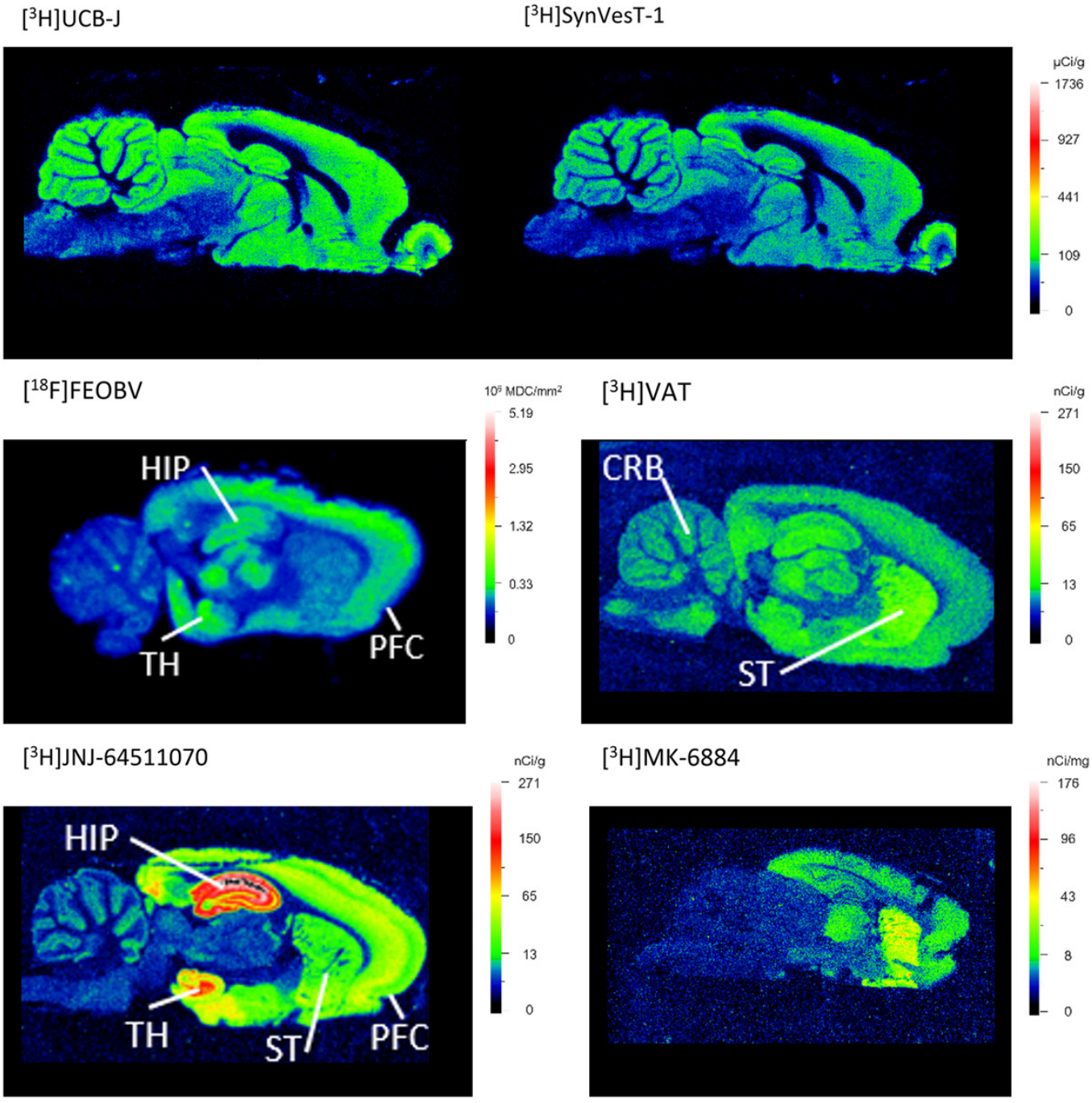

Figure S1. Total binding in sagittal sections of a healthy rat brain for [^{3}H]UCB-J and [^{3}H]SynVesT-1, [^{18}F]FEOBV, [^{3}H]VAT, [^{3}H]JNJ-64511070, and [^{3}H]MK-6884; HIP = hippocampus, TH = thalamus, PFC = prefrontal cortex, CRB = cerebellum, ST = striatum.

Distribution in post-mortem human tissues

Demographic data for the postmortem brain samples

Postmortem human samples were obtained from Eisai Inc. Information regarding the age of the subjects, as well as brain regions provided (cerebellum = CRB, prefrontal cortex = PFC, and hippocampus = HIP) are summarized in **Table 1** of the main paper. The sample size included two females and three males with AD, two females and one male with MCI and three females NHV.

Cerebellum

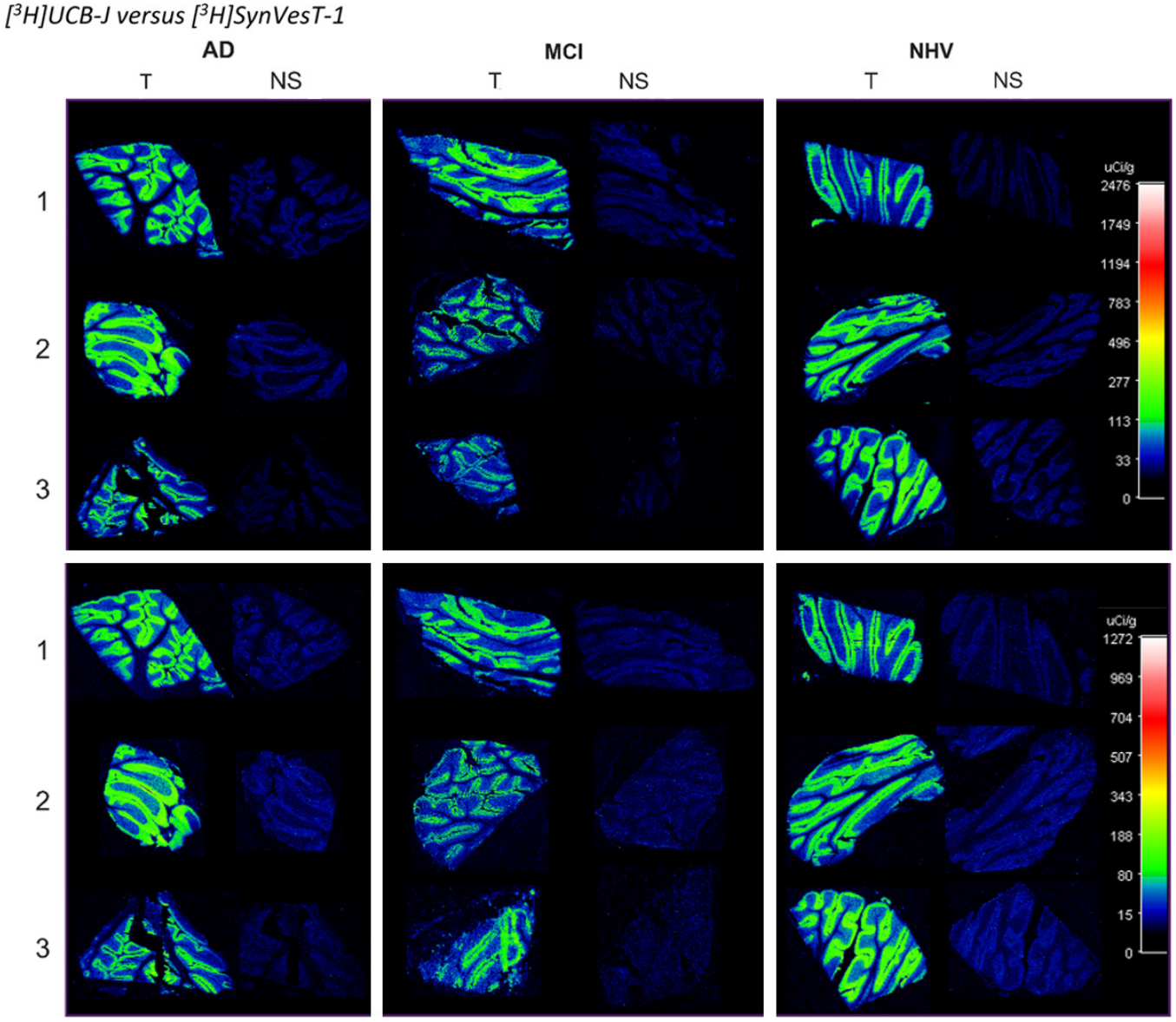

Figure S2. Total (T) and non-specific (NS) binding in cerebellum sections of AD, MCI and NHV tissues for [^{3}H]UCB-J (top) and [^{3}H]SynVesT-1 (bottom).

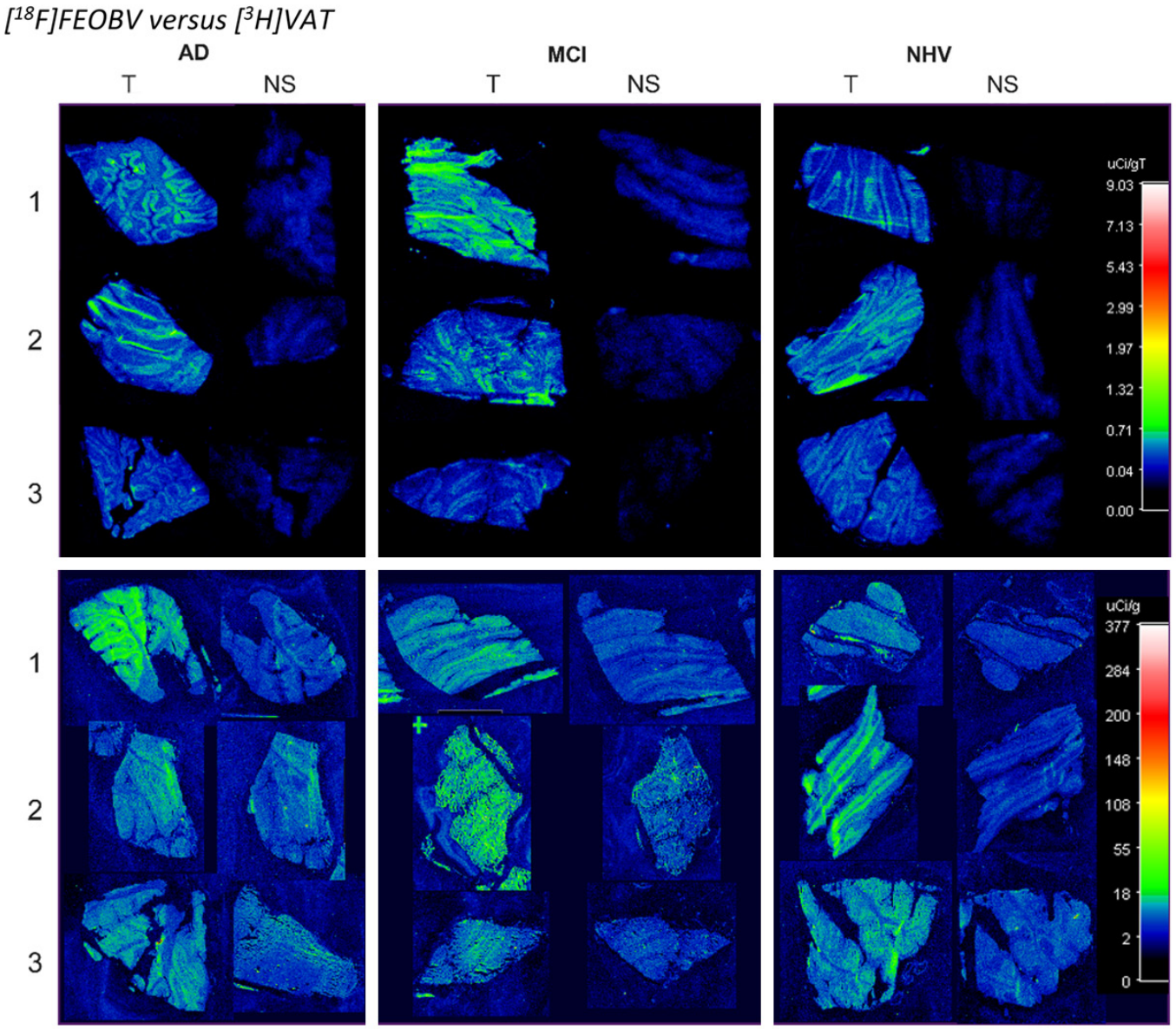

Figure S3. Total (T) and non-specific (NS) binding in cerebellum sections of AD, MCI and NHV tissues for [^{18}F]FEOBV (top) and [^{3}H]VAT (bottom).

[^{3}H]JNJ-64511070

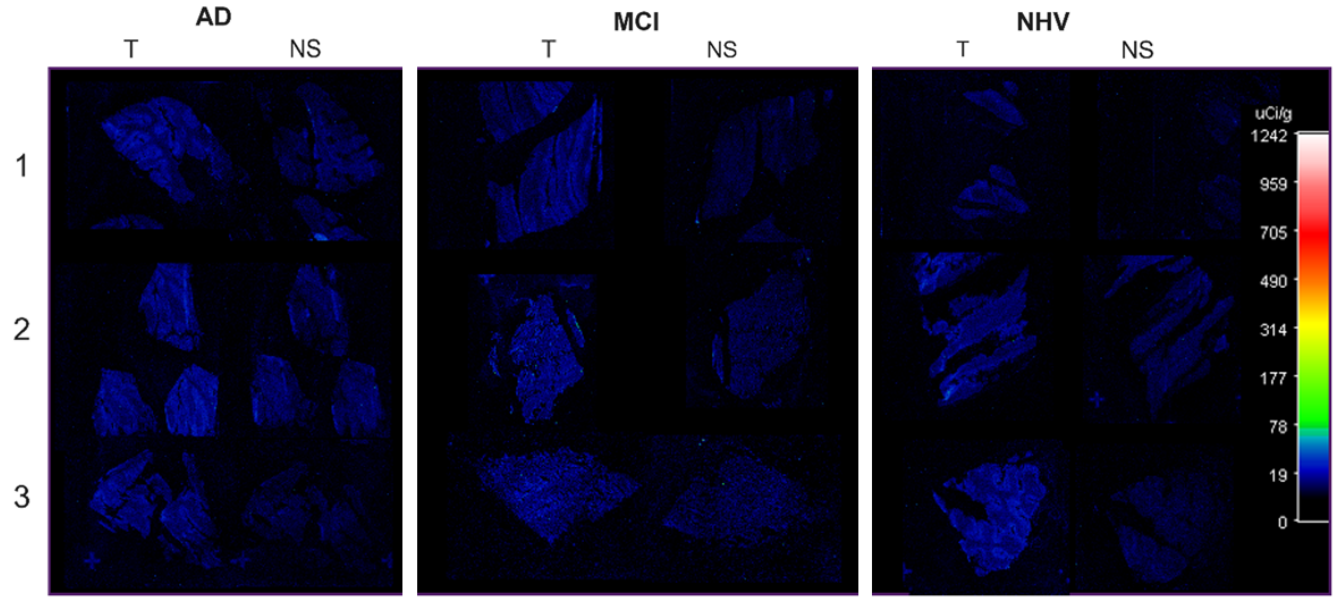

Figure S4. Total (T) and non-specific (NS) binding in cerebellum sections of AD, MCI and NHV tissues for [^{3}H]JNJ-64511070.

[^{3}H]MK-6884 + 10 µM carbachol

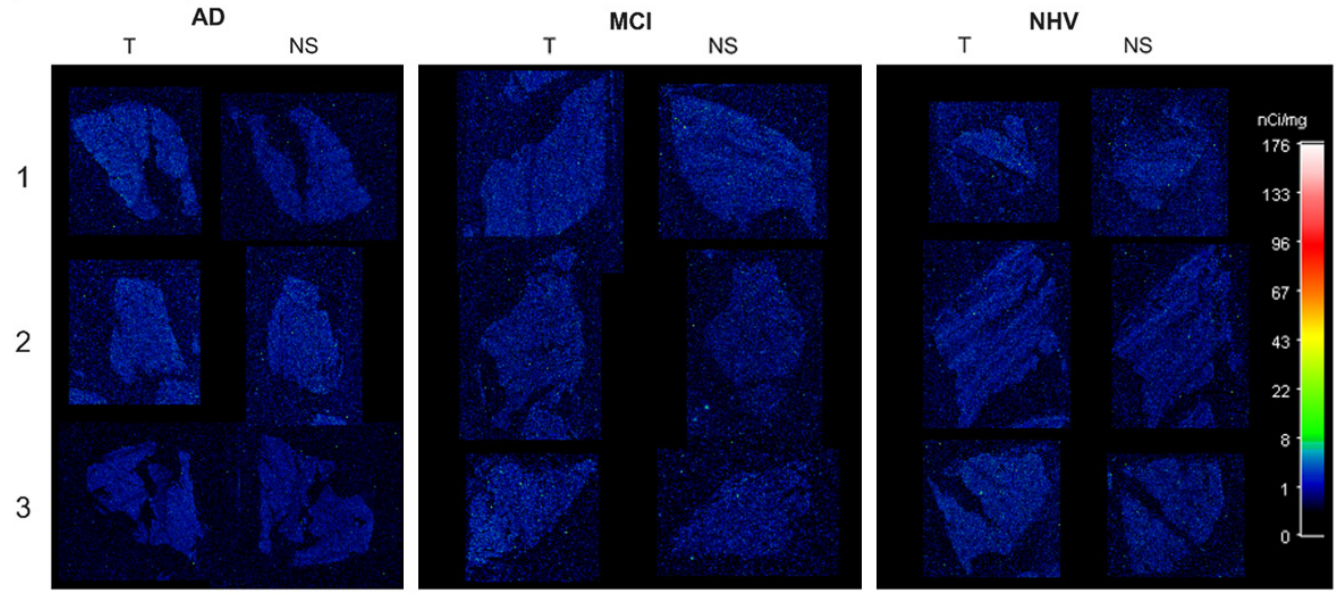

Figure S5. Total (T) and non-specific (NS) binding in cerebellum sections of AD, MCI and NHV tissues for [^{3}H]MK-6884 + 10 µM carbachol.

Prefrontal cortex

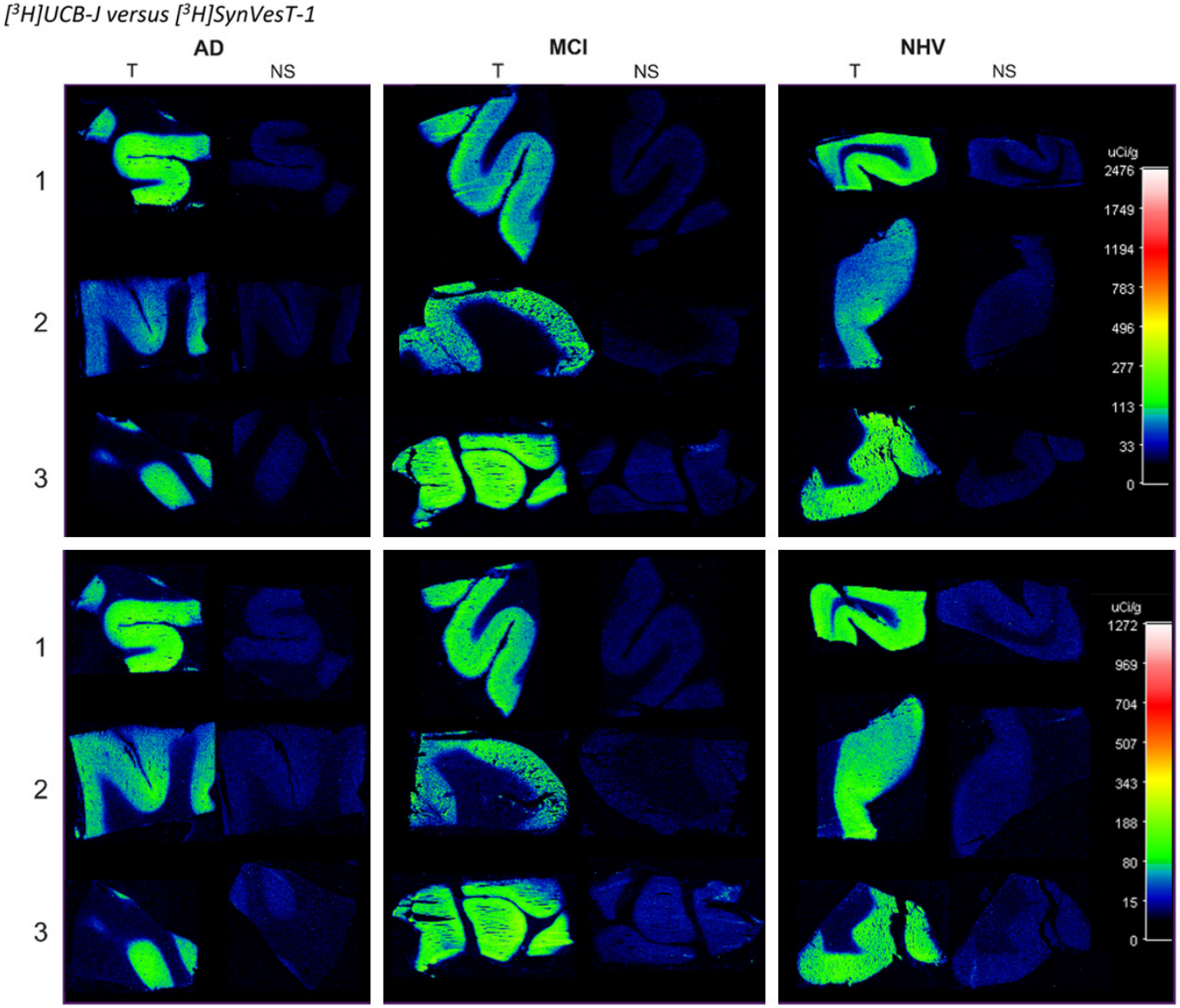

Figure S6. Total (T) and non-specific (NS) binding in prefrontal cortex sections of AD, MCI and NHV tissues for [^{3}H]UCB-J (top) and [^{3}H] SynVesT-1 (bottom).

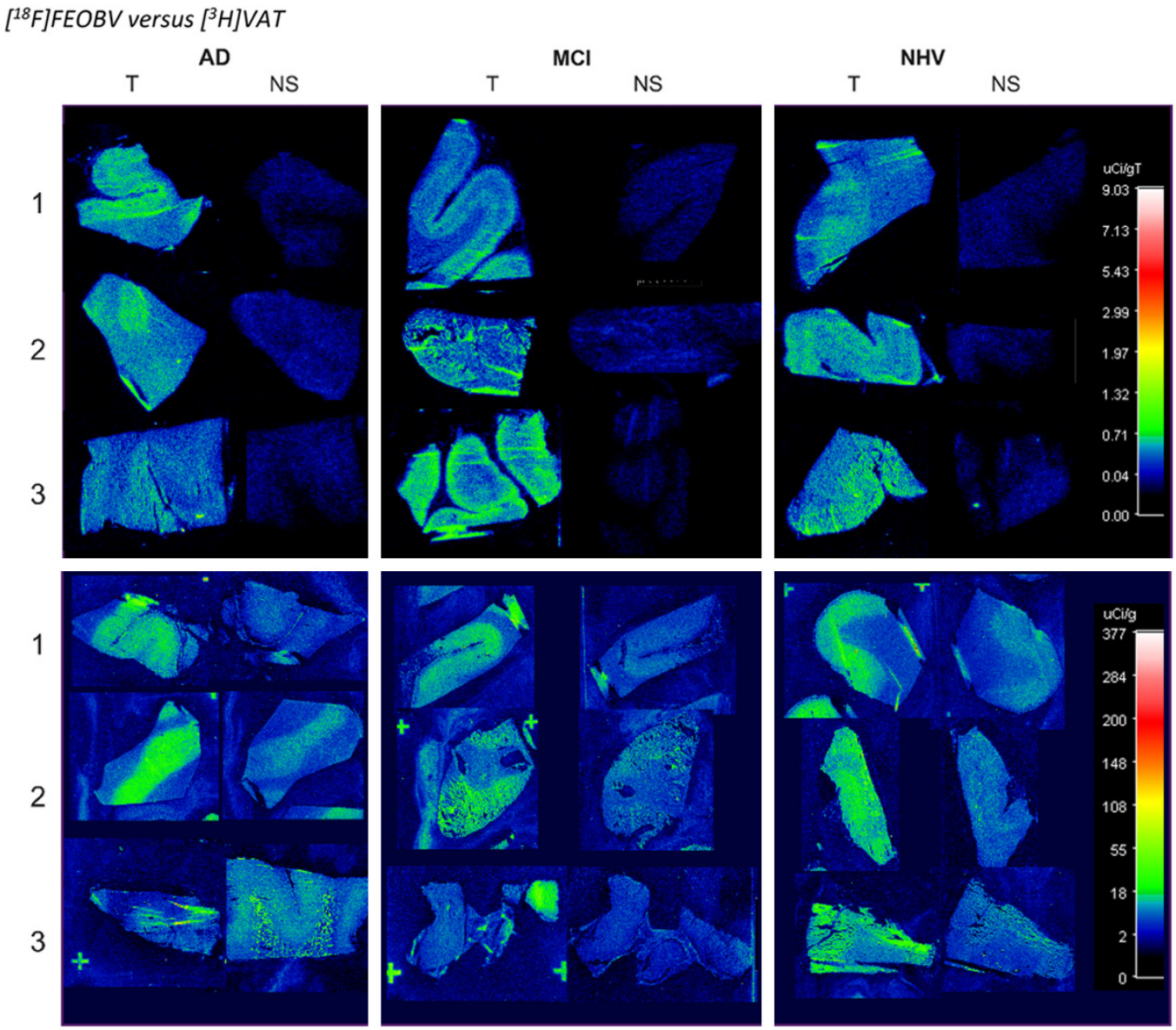

Figure S7. Total (T) and non-specific (NS) binding in prefrontal cortex sections of AD, MCI and NHV tissues for [^{18}F]FEOBV (top) and [^{3}H]VAT (bottom).

[^{3}H]JNJ-64511070

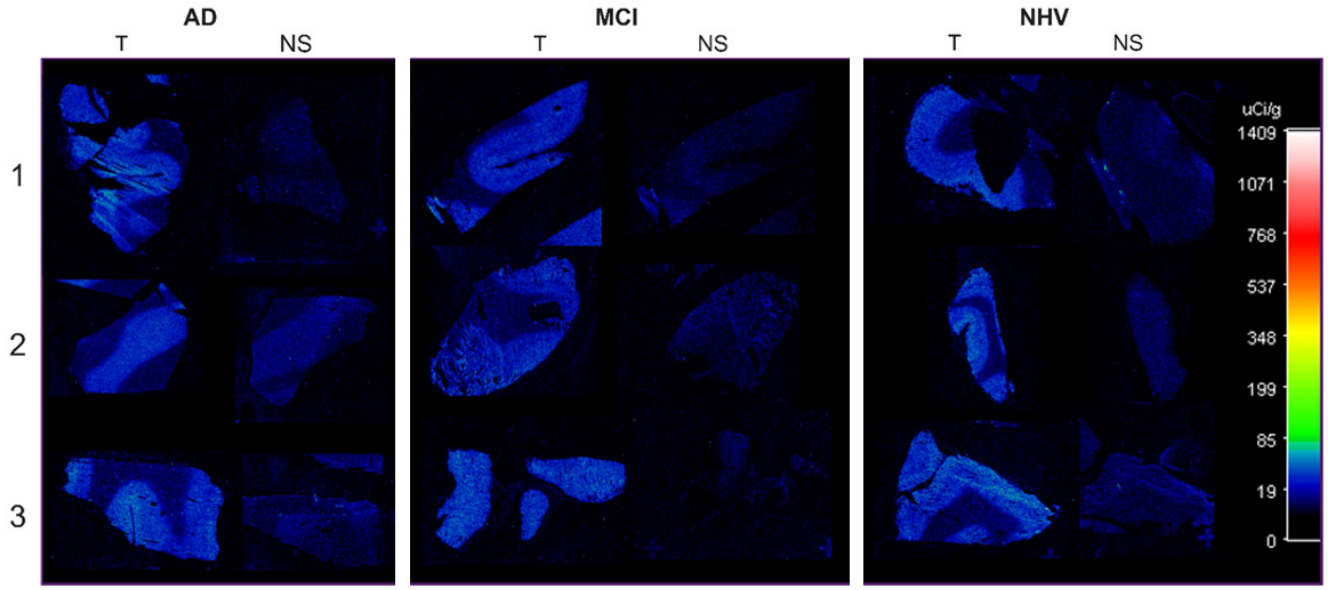

Figure S8. Total (T) and non-specific (NS) binding in prefrontal sections of AD, MCI and NHV tissues for [^{3}H]JNJ-64511070.

[^{3}H]MK-6884 + 10 μM carbachol

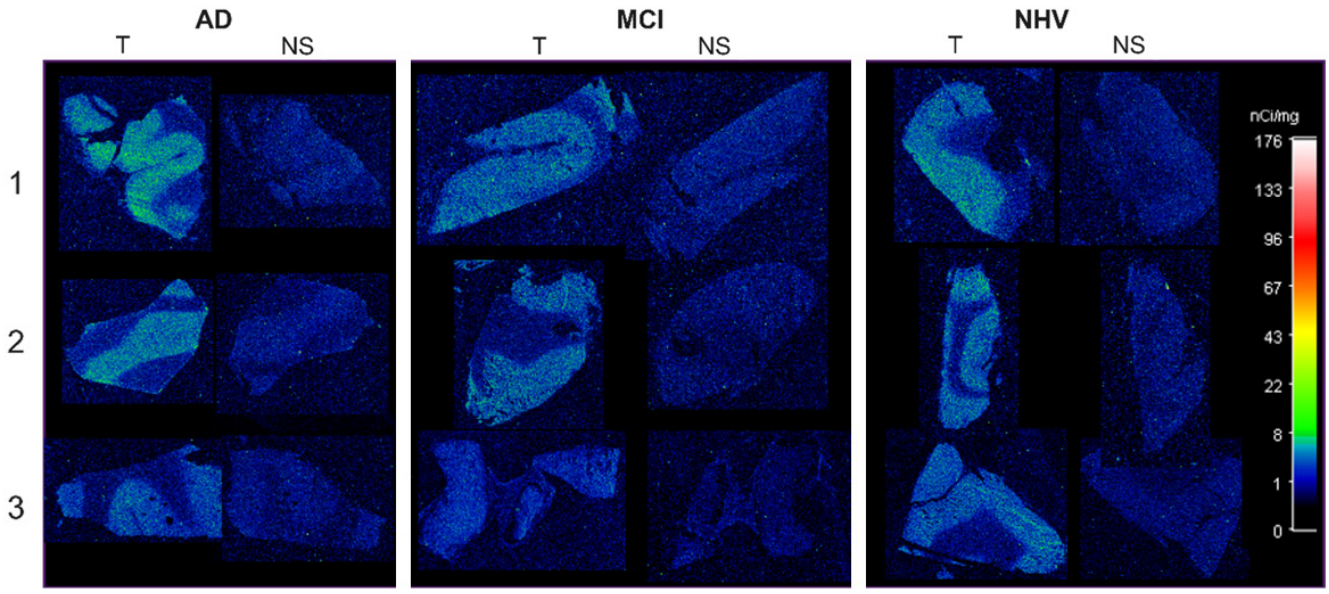

Figure S9. Total (T) and non-specific (NS) binding in prefrontal sections of AD, MCI and NHV tissues for [^{3}H]MK-6884 + 10 μM carbachol.

Hippocampus

[^{3}H]UCB-J versus [^{3}H]SynVesT-1

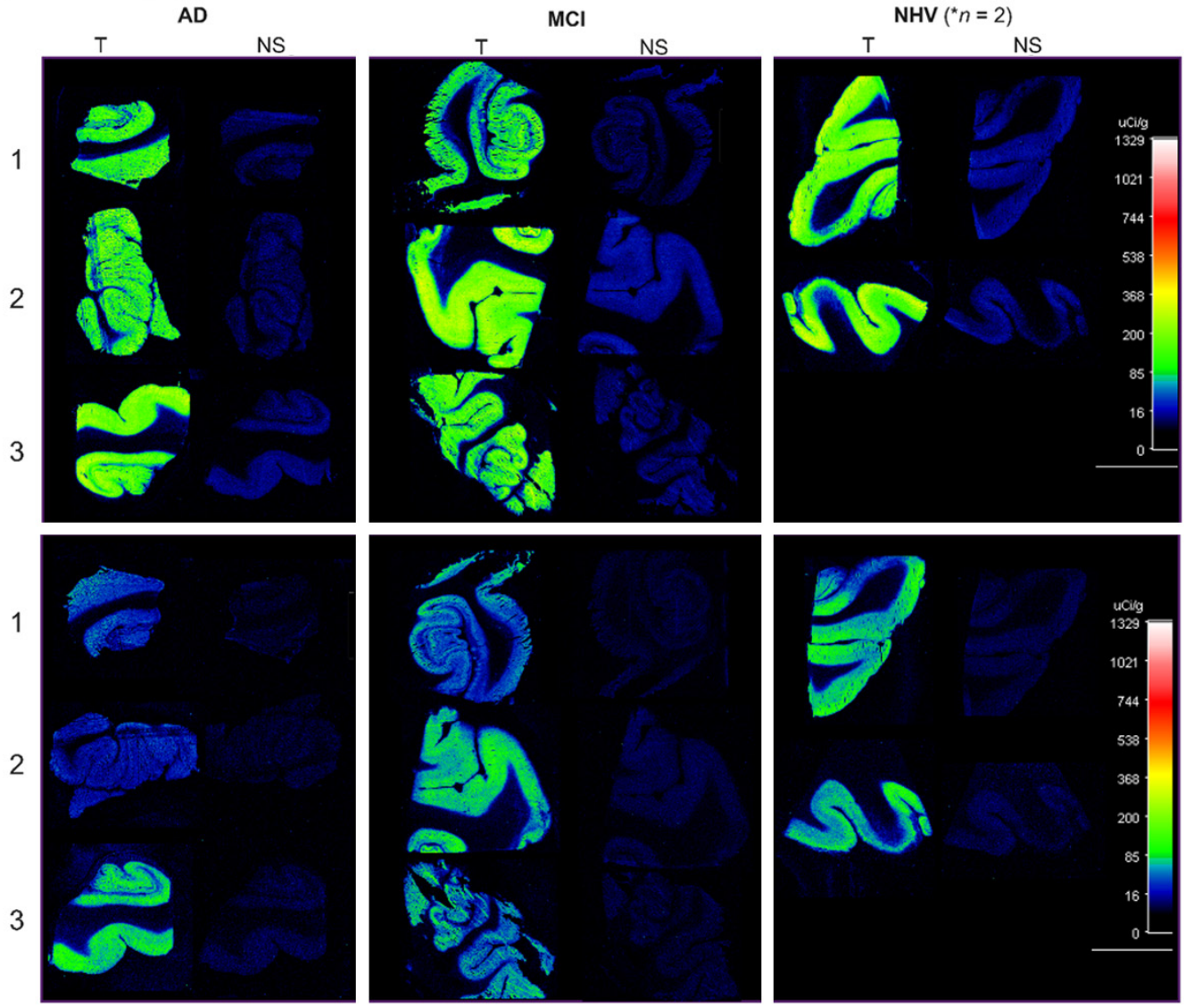

Figure S10. Total (T) and non-specific (NS) binding in hippocampus sections of AD, MCI and NHV tissues for [^{3}H]UCB-J (top) and [^{3}H] SynVesT-1 (bottom).

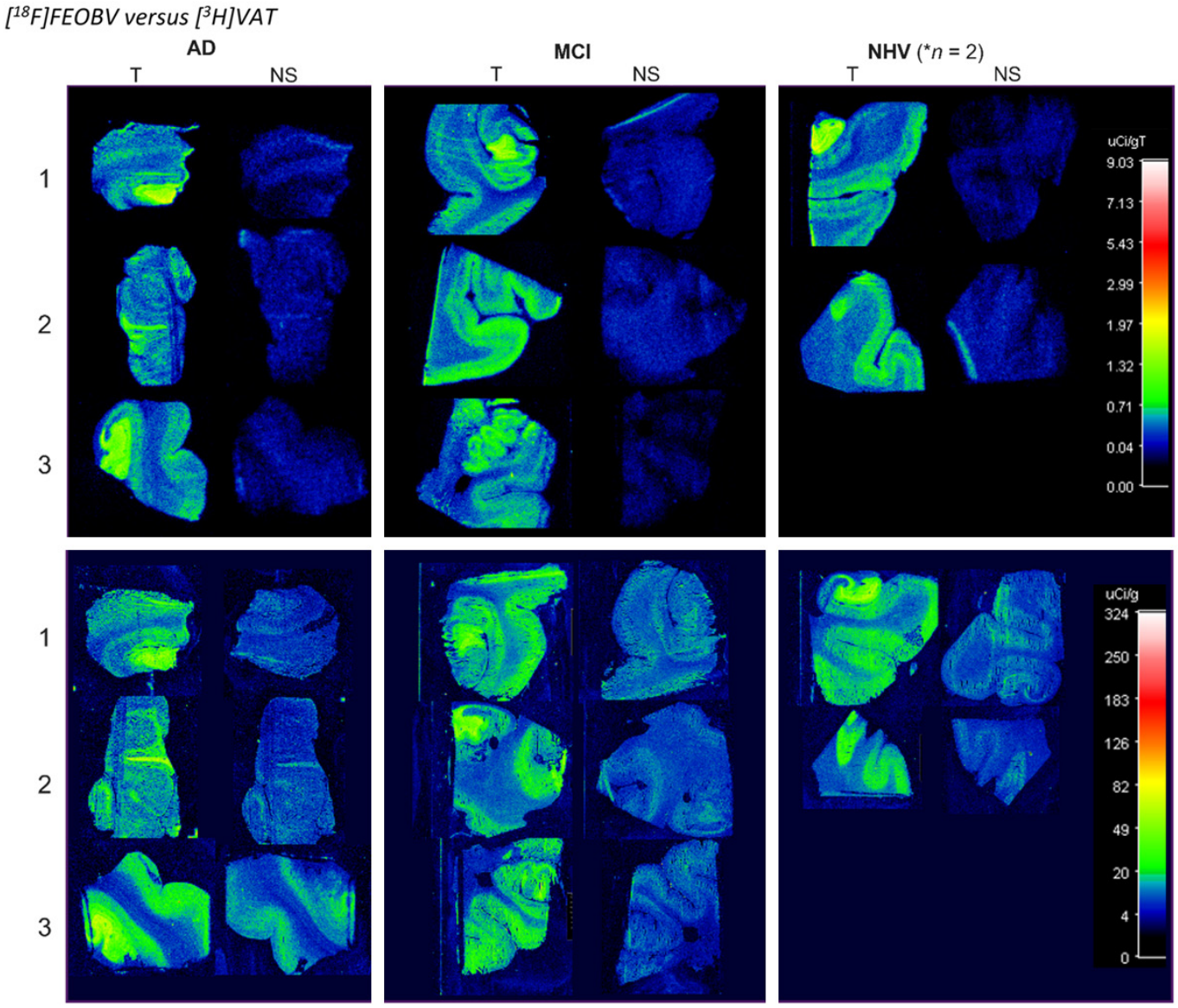

Figure S11. Total (T) and non-specific (NS) binding in hippocampus sections of AD, MCI and NHV tissues for [^{18}F]FEOBV (top) and [^{3}H] VAT (bottom).

[^{3}H]JNJ-64511070

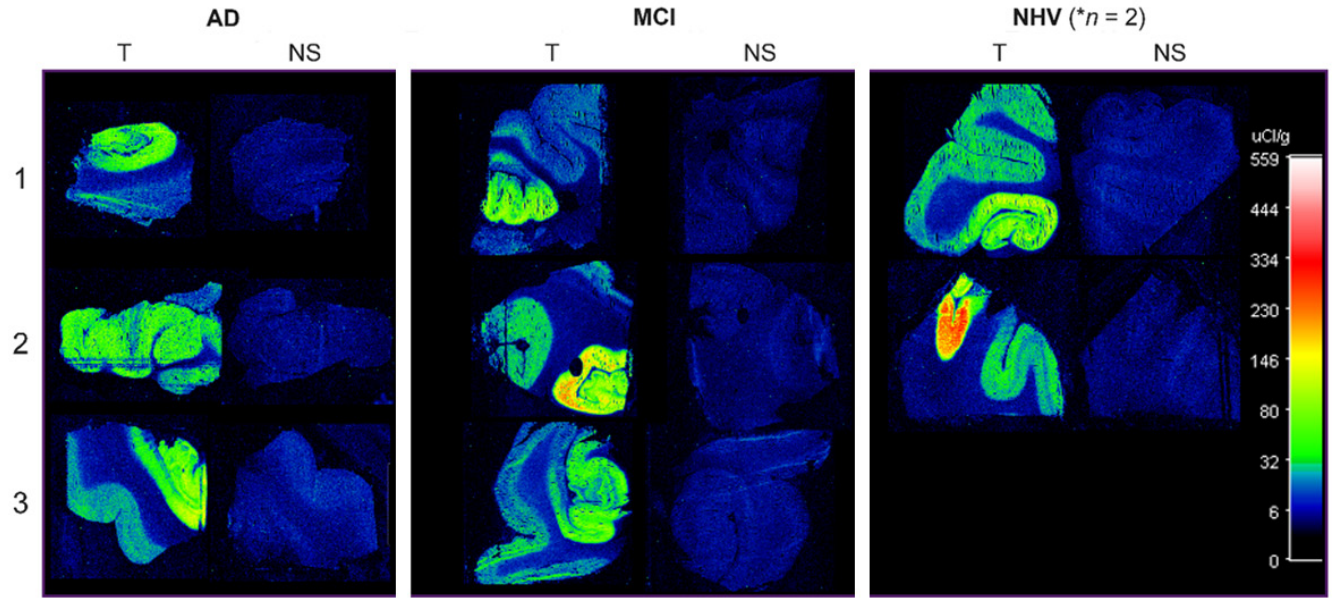

Figure S12. Total (T) and non-specific (NS) binding in hippocampus sections of AD, MCI and NHV tissues for [^{3}H]JNJ-64511070.

[^{3}H]MK-6884 + 10 μM carbachol

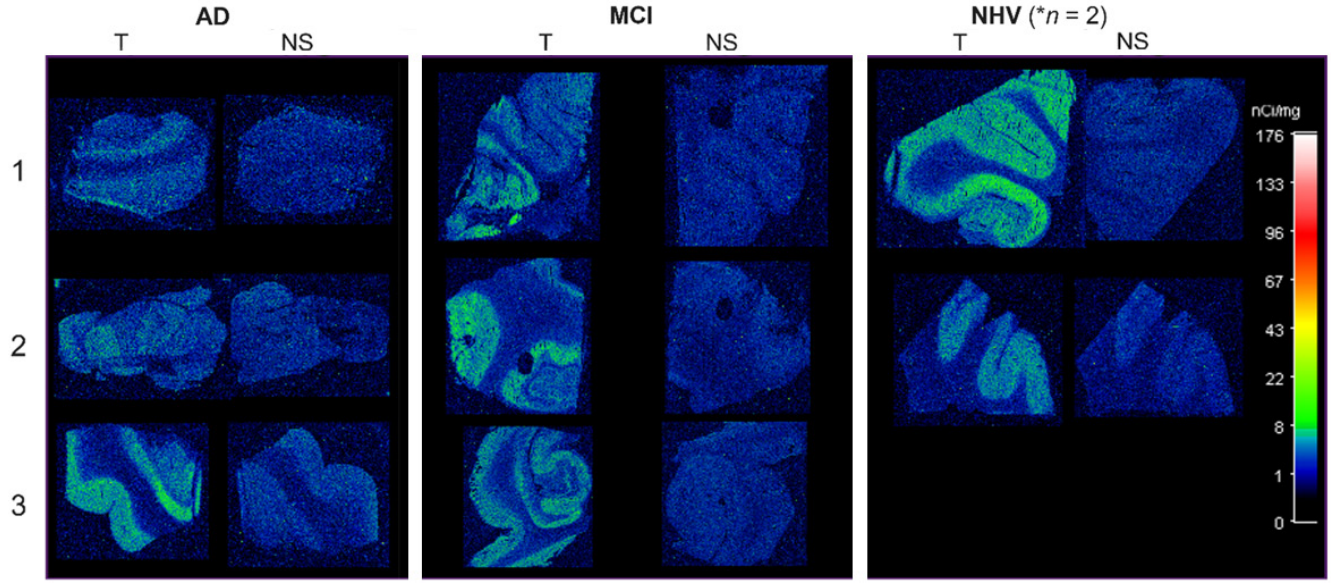

Figure S13. Total (T) and non-specific (NS) binding in hippocampus sections of AD, MCI and NHV tissues for [^{3}H]MK-6884 + 10 μM carbachol.